Novel Origins and Proliferative States of Human Oligodendrocyte Precursor Cells

Wei Huang[1,2,8,*], Aparna Bhaduri[1,2,8], Dmitry Velmeshev[1,2], Shaohui Wang[1,2], Li Wang[1,2], Catherine A. Rottkamp[1,3], Arturo Alvarez-Buylla[1,4], David H. Rowitch[1,5,6,7], and Arnold R. Kriegstein[1,2,9]*

[1]The Eli and Edythe Broad Center of Regeneration Medicine and Stem Cell Research, University of California, San Francisco (UCSF), San Francisco, CA 94143, USA

[2]Department of Neurology, UCSF, San Francisco, CA 94143, USA

[3]Present Address: Department of Pediatrics, UC Davis Children's Hospital, Sacramento, CA 95817, USA

[4]Department of Neurological Surgery, UCSF, San Francisco, CA 94143, USA

[5]Departments of Pediatrics and Neurosurgery, UCSF, San Francisco, CA 94143, USA

[6]Department of Paediatrics, University of Cambridge, Cambridge, CB2 0QQ, UK

[7]Wellcome - MRC Cambridge Stem Cell Institute, University of Cambridge, Cambridge, CB2 0QQ, UK

[8]These authors contributed equally

[9]Lead Contact

*Correspondence: arnold.kriegstein@ucsf.edu (A.R.K.), wei.huang@ucsf.edu (W.H.)

Graphical Abstract

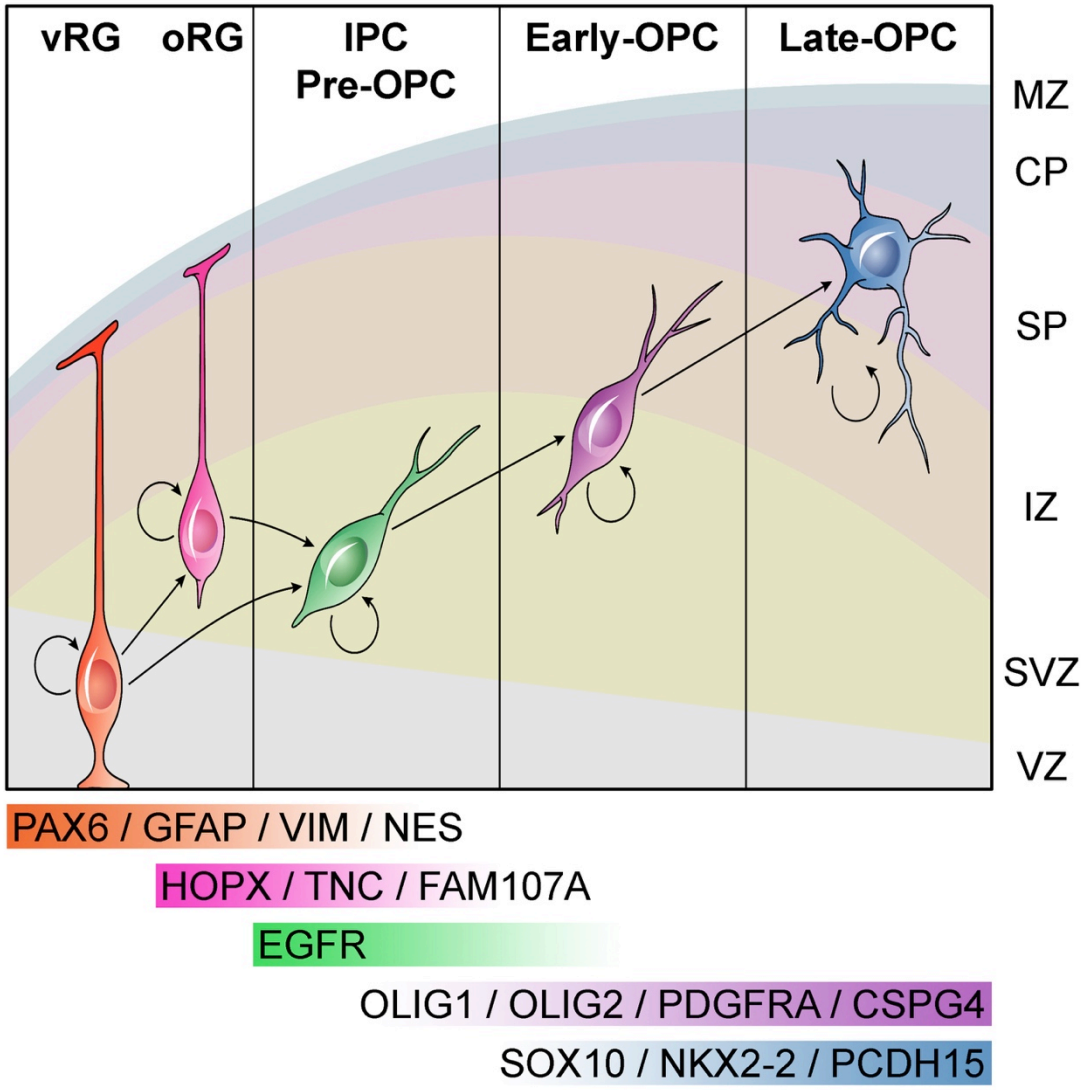

Highlights

- **Human oRGs are an additional source to generate OPCs through Pre-OPCs**
- **Pre-OPCs express EGFR and undergo a hybrid mitotic somal translocation during division**
- **OPCs undergo consecutive symmetric divisions to exponentially increase the progenitor cell pool**
- **OPC enriched PCDH15 mediates daughter cell repulsion and facilitates proliferation**

SUMMARY

The human cerebral cortex has enlarged greatly during evolution, with expanded grey and white matter volumes. While increased progenitor diversity and enhanced proliferative potential play important roles in human neurogenesis and grey matter expansion, the mechanisms of human oligodendrogenesis and white matter expansion remain largely unknown. Here we identify novel EGFR-expressing intermediate progenitor cells (Pre-OPCs) that originate from outer radial glial cells (oRGs) and undergo mitotic somal translocation (MST) during division. They produce oligodendrocyte precursor cells (OPCs), providing an additional source of human cortical OPCs and defining a unique trajectory of oligodendrogenesis. We further demonstrate that OPCs undergo consecutive symmetric divisions to exponentially increase the progenitor cell pool. Finally, we find that the OPC enriched gene, *PCDH15*, mediates daughter cell repulsion and facilitates proliferation. These findings indicate properties of OPC derivation, proliferation, and dispersion in the developing human brain that contribute to white matter expansion.

KEYWORDS

outer radial glia (oRG), intermediate progenitor cell (IPC), oligodendrocyte precursor cell (OPC), oligodendrogenesis, cortical expansion, *EGFR*, *PCDH15*, self-repulsion, homeostasis

INTRODUCTION

Cerebral white matter has enlarged dramatically during evolution, associated with a significant increase in myelinating oligodendrocytes which are the major white matter cell type (Zhang and Sejnowski, 2000; Simons and Nave, 2015). However, most of our knowledge of oligodendrocyte development is derived from animal studies (Fancy et al., 2011; Bergles and Richardson, 2015; Emery and Lu, 2015) and relatively little is known about the distinct features of human oligodendrocyte production and how its regulation contributes to human white matter expansion.

In rodents, oligodendrocytes arise from the differentiation of oligodendrocyte precursor cells (OPCs), which are derived from embryonic progenitors near the ventricle (Warf et al., 1991; Pringle and Richardson, 1993; Cai et al., 2005; Fogarty et al., 2005; Vallstedt et al., 2005). In the mouse forebrain, OPCs are generated in three successive waves from the ganglionic eminences and the cortical ventricular zone (Kessaris et al., 2006). In the human brain, the first PDGFRA-expressing OPCs appear around 10 gestational weeks (GW10). Their numbers increase at GW15 and are mainly found in the ganglionic eminences and cortical germinal zones, reflecting an evolutionary conservation of OPC production at sites surrounding the ventricles (Jakovceviki and Zecevic, 2005; Rakic and Zecevic, 2003; Mo and Zecevic, 2009). However, primates develop an enlarged cortical germinal zone, the outer subventricular zone (OSVZ), which is lacking in most rodents (Smart et al., 2002; Zecevic et al., 2005; Fish et al., 2008), and diverse progenitors in the OSVZ contribute to neurogenesis and the enlargement of the human cerebral cortex (Betizeau et al., 2013; Nonako-Kinoshita et al., 2013). It is unclear whether there are any additional progenitor sources of human OPC production associated with white matter expansion and how human OPCs enhance oligodendrocyte production to match the increase demands for myelination.

Here we investigate the origin of human cortical OPCs and characterize the trajectory of OPC production. Combining single-cell RNA-sequencing (scRNA-seq), immunohistochemistry, immunopanning, primary cell and brain slice culture, as well as time-lapse imaging, we identify a novel intermediate progenitor cell type, the EGFR-expressing Pre-OPC, present at the onset of gliogenesis in the OSVZ. These highly proliferative cells exhibit unique dividing dynamics

characterized by a diminutive mitotic somal translocation (MST) and produce OPCs. We also provide evidence that outer radial glial cells (oRGs) support oligodendrogenesis, providing an extra source of OPC production in the human cortex that has not been observed in rodents. We further demonstrate that human OPCs in the OSVZ undergo frequent consecutive symmetric divisions to amplify progenitor cell number exponentially and describe a unique repulsive behavior between OPC daughter cells mediated by the OPC-enriched gene *PCDH15*. The latter serves to avoid local OPC accumulation and facilitate OPC proliferation. These findings highlight a novel oligodendrocyte lineage in the human brain with enhanced precursor proliferation and a mechanism for cell dispersion, deepening our understanding of human oligodendrogenesis and cortical expansion.

RESULTS

Transcriptional Profiles of OPCs in the Developing Human Cortex

In order to study the diversity and developmental trajectories of human OPCs, we sought to survey their transcriptional profiles in the developing cortex by scRNA-seq (Figure 1A). We previously applied scRNA-seq to generate a census of the main cell types in the developing human cortex, including neural progenitor cells (NPC), intermediate progenitor cells (IPC), neurons, astrocytes, oligodendrocytes, microglia, and endothelial cells (Nowakowski et al., 2017). However, among the 4,261 unbiased captured cells, only 40 were OPCs (Figure 1B), possibly due to low abundance during the late first and second trimester and high fragility.

Unlike studies in mouse, where transgenic lines and fluorescence-activated cell sorting (FACS) of GFP labeled OPCs (eg: *PDGFRA*-H2B-*GFP*) have been used for scRNA-seq (Marques et al., 2016 and 2018), a transgenic strategy is not possible with human samples. To study human OPCs during the onset of gliogenesis, we leveraged immunopanning techniques (Dugas and Emery, 2013; Barres, 2014) to enrich for OPCs (Figure 1A). Primary cortical cells were dissociated from nine brain samples at GW20-GW24 and cells expressing PDGFRA were collected using PDGFRA-antibody coated petri dishes. Post-staining showed that most of the immunopanned cells were PDGFRA^{+}NKX2-2^{+} and scRNA-seq showed that the majority of the immunopanned cells expressed *PDGFRA* mRNA (Figure 1C), indicating high efficiency of OPC enrichment. When we combined these PDGFRA-immunopanned cells with our previous

4,261 unbiased captured cells and clustered them by principle component analysis (PCA) and Louvain-Jaccard clustering, a total of 980 high quality cells were characterized as OPCs according to their RNA profiles (Figure 1D). Differential gene expression analysis showed that these cells expressed conventional OPC genes *OLIG1*, *OLIG2*, *PDGFRA*, *NKX2-2*, *SOX10*, *S100B*, and *APOD* (Figure 1E). Conversely, they did not express neuronal lineage genes *EOMES*, *PPP1R17*, *NEUROD2*, or *NEUROD6*, and were also well separated from clusters of IPCs, excitatory neurons (EN), and interneurons (IN) (Figure 1F).

The OPCs were clustered into four groups (clusters 14, 2, 20, and 11). Metadata annotation showed that cortical OPCs acquired by unbiased-capture were mixed evenly with OPCs enriched by PDGFRA-immunopanning and major groups were composed of cells from multiple individuals (Figure 2A), indicating minimal effects of technical artifacts and batch differences. Cluster 20 included the largest number of PDGFRA-immunopanned cells (Figure 2A) and cluster 11 expressed cell cycling genes *MKI67*, *ASPM*, *TOP2A*, and *CDK1*, indicating that these OPCs were actively dividing (Figure 2B). Cluster 2 was close to cluster 20 based upon gene expression similarity analysis, so these two clusters might reflect OPCs at different maturation states.

Interestingly, we found that cluster 14 expressed low levels of NPC genes, including *GFAP*, *VIM*, *NES*, *HES1*, *NOTCH2*, and *EGFR* (Figure 2B). In contrast, oligodendrocyte lineage genes *OLIG1*, *OLIG2*, and *PDGFRA* were also relatively low in this cluster compared with other OPC clusters, and later stage OPC genes like *NKX2-2*, *SOX10* and *APOD* were not expressed (Figure 2B). Metadata analysis showed that cluster 14 was mainly composed of cells micro-dissected from the cortical germinal zone (Cortex-VZ/SVZ) (Figure 2A). Similarity analysis indicated that cluster 14 was closely related to both NPCs and OPCs (Figure 2C), suggesting a transitional Pre-OPC stage from multi-potent NPCs to lineage committed OPCs. This was supported by a trajectory reconstruction based upon our scRNA-seq by monocle (Trapnell et al., 2014; Qiu et al., 2017) (Figure 2D and 2E). According to the pseudo-lineage tree, *VIM*-expressing NPCs could generate *EOMES*-expressing IPCs that further differentiate into *NEUROD6*-expressing neurons. However, a branch point just prior to neurogenic IPC generation suggested that NPCs could also generate Pre-OPCs that further differentiated into

other OPC clusters (Figure 2D). Feature plots showed NPC genes like *VIM* and *GFAP* were down-regulated upon lineage commitment, while OPC genes like *PDGFRA* and *APOD* were up-regulated (Figure 2E). Together, our scRNA-seq analysis suggests a local intermediate progenitor source supporting OPC generation in the human cortex.

EGFR-expressing Cells as Novel Intermediate Progenitors for Oligodendrogenesis

ScRNA-seq analysis has indicated that mouse oligodendrocytes progress through various stages of differentiation (Marques et al., 2016 and 2018), but the progenitor types and developmental trajectory that generate OPCs prior to lineage commitment remain unclear. We were also interested in exploring any potential links between neurogenesis and oligodendrogenesis. In order to address these questions, we first used immunohistochemistry to characterize OPCs in second trimester fixed human cortical brain sections (Figure S1). We found that $PDGFRA^{+}OLIG2^{+}$ OPCs were present in low numbers across all cortical laminae and were distributed radially from the ventricular zone (VZ) to the cortical plate (CP) during middle to late stages of neurogenesis (GW16 and GW18). The number of OPCs increased dramatically after GW20, and continued to increase at GW24, the latest age we studied.

We then evaluated cluster 14 OPCs by co-staining human cortical sections at GW20-24 for OPC and NPC markers. Most $PDGFRA^{+}OLIG2^{+}$ OPCs did not express NPC markers, but more than 10% of OPCs expressing low levels of PDGFRA and OLIG2 co-expressed NPC markers, NES, GFAP, VIM, and EGFR, reflecting an NPC signature (Figure 3A and S2). However, these $EGFR^{+}PDGFRA^{+}$ cells also expressed other OPC markers, OLIG1 and NG2, supporting a commitment to the oligodendrocyte lineage (Figure 3A). Moreover, the co-labeled cells had bipolar morphology, consistent with an immature OPC stage. Distribution analysis showed that most $EGFR^{+}PDGFRA^{+}OLIG2^{+}$ cells were located in the OSVZ, though some were also present in the inner subventricular zone (ISVZ) and intermediate zone (IZ) (Figure S2). Considering their NPC and OPC marker co-expression, immature bipolar morphology, and germinal zone location, we reasoned that these cells might represent a transitional stage from NPCs to OPCs, consistent with our scRNA-seq data (Figure 2).

We next sought to determine the NPC subtypes that are capable of generating OPCs. Differential gene analysis based on scRNA-seq showed that EGFR was enriched in cluster 14 (Figure 2B) and expressed in a subpopulation of NPCs (Figure 2E). In normal development, EGFR signaling regulates oligodendrogenesis and myelination in both juvenile and adult mice (Aguirre et al., 2007). Here, in late second trimester (GW20-24) at the onset of gliogenesis, we found a large population of $EGFR^{+}OLIG2^{+}$ cells in the germinal zones of the cortex. These cells were present in the cortex at low abundance at GW16 and GW18 but increased dramatically between GW20 and GW24 (Figure S3), coinciding with OPC generation (Figure S1). They were highly proliferative, with approximately 50% of $EGFR^{+}OLIG2^{+}$ cells expressing KI67 at GW20, and were mainly located in the OSVZ (Figure S3). The EGFR+ cells in the germinal zone also expressed NES and SOX2. We next asked whether the EGFR-expressing cells were subtypes of oRGs or IPCs, the two major types of neurogenic progenitors in the OSVZ. Unlike oRGs that exhibit a long radial process, EGFR-expressing cells were found randomly oriented in the germinal zone, being vertical, oblique or even horizontal to the ventricular surface (Figure S2-S4). Most EGFR+OLIG2+ cells did not express pS6 (Figure 3B), an oRG marker and a canonical readout of activated mTOR signaling (Nowakowski et al., 2017). Conversely, most $TNC^{+}SOX2^{+}$ oRGs in the OSVZ did not express EGFR (Pollen et al., 2015) (Figure 3B). These results suggest that EGFR labels a population of progenitor cells in the OSVZ separate from oRGs. Additionally, we found that the $EGFR^{+}OLIG2^{+}$ cells never expressed neurogenic IPC markers, such as EOMES or PPP1R17, suggesting a lineage separation between oligodendrocytes and neurons (Figure 3B). Taken together, our *in vivo* immunohistochemistry findings suggest a novel intermediate progenitor type abundant in the OSVZ during gliogenesis that expresses EGFR.

We further tested whether the EGFR-expressing progenitors could generate OPCs. Cells were dissociated from the micro-dissected OSVZ at GW20 to GW24. OPCs were depleted from the cell suspension by two sequential rounds of PDGFRA- and O4-immunopanning to ensure that any OPCs produced later would be generated from precursor cells and not by OPC self-renewal (Figure 3C). Progenitor cells were further enriched through positive selection by EGFR-immunopanning. The EGFR-expressing non-OPC cells were cultured in EGF containing medium for two days and then in PDGF containing medium for five additional days, and fixed

at two days *in vitro* (DIV2) or seven days *in vitro* (DIV7). At DIV2, 90-96% of the cells were $EGFR^+$, suggesting high efficiency of the immunopanning-based enrichment strategy, and 23% were $OLIG2^+$, but none were $NG2^+$, $PDGFRA^+$, or $NKX2\text{-}2^+$, consistent with OPC depletion (Figure 3C). In contrast, by DIV7, the percentage of $EGFR^+$ cells had decreased to 40-48%, while the percentage of $OLIG2^+$, $PDGFRA^+$, $NG2^+$ and $NKX2\text{-}2^+$ cells had increased to 35%, 35%, 36% and 28%, respectively (Figure 3C). Reduction of EGFR-expressing progenitor cells accompanied the generation of OPCs, suggesting that $EGFR^+$ progenitors in the germinal zone of the cortex have the ability to produce OPCs.

We reasoned that if the EGFR-expressing cells were progenitors of OPCs, then manipulation of the EGFR signaling pathway might affect EGFR-expressing cell proliferation and ultimately change OPC production. To test this possibility, we cultured human brain slices at GW20-24, and treated adjacent slices with EGF, or with the EGFR inhibitors, Iressa, AG1478, or PD153035. Slices were incubated with BrdU for 12h before fixation at DIV7. In comparison with DMSO treated control slices, the number of both $OLIG2^+KI67^+$ and $NKX2\text{-}2^+BrdU^+$ cells increased by EGF treatment in a dose dependent manner, while both populations decreased dramatically when treated by all three of the EGFR inhibitors (Figure 3D). The decrease in OPC proliferation in the presence of EGFR inhibitors demonstrates that EGF endogenously activates OPC production in cortical slices. This result combined with the differentiation assay supports the concept of local generation of OPCs from EGFR-expressing progenitors in late second trimester human cortex.

oRGs as an Additional Source Generate OPCs in the Developing Human Brain

When we characterized OPCs in fixed human cortical sections by immunohistochemistry, we noticed that at GW20-24 the VZ did not contain many $PDGFRA^+OLIG2^+$ cells compared with other laminar regions (Figure S1). In contrast, the highest density of OPCs was found in the OSVZ, suggesting substantial OPC production in this region. During evolution, an increase in the diversity and number of progenitor cells within an enlarged OSVZ is thought to contribute to cortical expansion (Rakic 2009; Lui et al., 2011; Taverna et al., 2014; Fernandez et al., 2016). Our *in vivo* immunohistochemistry data outlined above show that both $PDGFRA^+OLIG2^+KI67^+$ OPCs and $EGFR^+OLIG2^+KI67^+$ Pre-OPCs were mainly located in the

OSVZ (Figure S1 and S3), suggesting a local source of OPC production in the OSVZ. Neurogenic oRGs are a subtype of radial glia found in the primate OSVZ that are rare in rodents and are thought to contribute to developmental and evolutionary grey matter expansion (Hansen et al., 2010; Fietz et al., 2010). However, the mechanisms underlying white matter expansion remain unknown, and whether oRGs are involved in human gliogenesis has not been fully demonstrated. Here, through differential gene expression analysis based on scRNA-seq data of human OPCs, we found that the Pre-OPC cluster (cluster 14) identified above also expressed the oRG genes *PTPRZ1*, *TNC*, *MOXD1*, *HOPX*, and *FAM107A* (Pollen et al., 2015) (Figure 2B), suggesting that oRGs might generate OPCs in the developing human cortex.

To validate the presence of a population of oRG marker-expressing OPCs in the human brain, we performed immunohistochemistry of fixed cortical sections between GW20 and GW24. We found that fewer than 2% of $PDGFRA^{+}OLIG2^{+}$ cells co-expressed the oRG markers, HOPX, PTPRZ1, TNC, and pS6 (Figure S4A). Moreover, these oRG marker-expressing OPCs exhibited immature bipolar morphology, and were mainly located in the ISVZ and OSVZ in the late second trimester. However, these cells were far less numerous than contemporaneous $EGFR^{+}PDGFRA^{+}OLIG2^{+}$ cells (Figure 3A and Figure S2). Given that we characterized EGFR-expressing cells as intermediate progenitors for OPCs, we think that oRGs might generate OPCs indirectly through oligodendrogenic IPCs (Pre-OPCs). Thus, we co-stained EGFR-expressing cells with oRG markers. We already showed that most $EGFR^{+}OLIG2^{+}$ cells did not express the active mTOR readout and oRG marker pS6, and most $TNC^{+}Sox2^{+}$ oRGs did not express EGFR either (Figure 3B), but we found that about 10% of $PTPRZ1^{+}SOX2^{+}$ oRGs in the OSVZ expressed EGFR, and nearly 20% of $EGFR^{+}OLIG2^{+}$ progenitors were co-labeled with the oRG marker HOPX (Figure S4B). This indicated that the expression time windows of different oRG markers might be slightly different from one another, and that some of oRG progeny still retain oRG marker expression, enabling lineage tracing and trajectory reconstruction. Distribution analysis of fixed cortical sections at GW22 revealed that the $HOPX^{+}EGFR^{+}OLIG2^{+}$ cells were mainly located in the OSVZ (Figure S5), consistent with the possibility that they represent a transitional stage from oRG to Pre-OPC. This would suggest that oRGs might be the precursors of EGFR-expressing intermediate progenitors that produce

OPCs. This concept is supported by our lineage trajectory reconstruction in which *HOPX*$^{+}$*TNC*$^{+}$ oRGs were positioned at the beginning of the pseudo-lineage tree. The lineage continued with *VIM*$^{+}$*EGFR*$^{+}$ progenitors that further branched into *EOMES*$^{+}$ neurogenic IPCs or *OLIG2*$^{+}$ Pre-OPCs (Figure 2D and 2E).

We further sought to directly test whether HOPX-expressing oRGs could generate OPCs. Cells were dissociated from the micro-dissected OSVZ at GW20 to GW24. Two sequential rounds of negative selection of (PDGFRA+O4)- and EGFR-immunopanning were performed in order to deplete both OPCs and Pre-OPCs in the cell suspension, and oRGs were further enriched through positive selection by LIFR-immunopanning as *LIFR* has been previously described as a marker of oRGs (Pollen et al., 2015). The LIFR-expressing progenitors were cultured in LIF containing medium for two days and then in EGF and PDGF containing medium for another eight days, and fixed at DIV2 and DIV10, respectively (Figure S4C). At DIV2, around 90% of the cells expressed SOX2, and more than 90% of the SOX2^{+} cells were GFAP^{+}HOPX^{+}, indicating oRG identity. None were PDGFRA^{+}, OLIG2^{+} or EGFR^{+}, consistent with OPC and Pre-OPC depletion (Figure S4C). In contrast, at DIV10, the percentage of SOX2^{+} cells decreased to 82%, and the percentage of GFAP^{+}HOPX^{+} cells decreased to 50%. Meanwhile, the percentage of EGFR^{+} cells increased to 44%, and the percentage of PDGFRA^{+}OLIG2^{+} cells increased to 17% (Figure S4C). Reduction of GFAP^{+}HOPX^{+}SOX2^{+} oRGs accompanied the generation of PDGFRA^{+}OLIG2^{+} OPCs, suggesting LIFR-antibody enriched oRGs are able to produce OPCs. The observation that nearly all the PDGFRA^{+}OLIG2^{+} OPCs generated at DIV10 also expressed EGFR indicates that oRGs generate OPCs through EGFR-expressing Pre-OPCs, consistent with the lineage reconstruction based on scRNA-seq analysis (Figure 2D and 2E). This differentiation assay combined with scRNA-seq and *in vivo* immunohistochemistry data indicate that a population of oRGs at the late second trimester act as neural progenitor cells for oligodendrogenesis. Our results also suggest that besides ventricular radial glia (vRG) present in both rodent and primate brain, the large abundance of oRGs in the developing human brain provides an extra source of OPC production absent in rodents, that could enhance oligodendrocyte generation and boost myelination to match demands arising from increased neurogenesis in the human brain.

Unique Division Dynamics of EGFR-expressing Progenitors in the OSVZ

Since EGFR-expressing cells appear to be intermediate progenitors that bridge oRGs and OPCs, we sought to study the proliferative behavior of these cells and compare them with the distinct mitotic behavior of oRGs and OPCs by time-lapse imaging. Due to the diversity of progenitors in the germinal zones at late second trimester and the lack of genetic tools to specifically label OPCs, EGFR-expressing IPCs, or oRGs, we dissociated cortical cells from OSVZ at GW20 to GW24 and performed immunopanning to selectively enrich specific progenitor populations through positive selection with PDGFRA-, EGFR-, and LIFR-antibody sequentially (Figure 4A). We subsequently labeled the individual enriched progenitor types by infecting them with *CMV-GFP* adeno-virus and transplanted the virus-labeled progenitors into the OSVZ of brain slices from the same tissue samples where the cells were derived. We then cultured the brain slices without adding any growth factors (Figure 4B). Since cultured slices largely preserve tissue integrity for at least one week in culture, including cortical layer structure (Noctor et al., 2001; Hansen et al., 2010), we reasoned that this experimental system could preserve many features of the *in vivo* niche supporting progenitor development.

To validate the identity of enriched cells, we performed 10X scRNA-seq of the immunopanned cells prior to virus infection and transplantation. Featured gene plots indicated a high efficiency of immunopanning. Most LIFR-panned cells highly expressed *LIFR*, and the major clusters were also enriched for *GFAP*, *PAX6*, *HOPX* and *PTPRZ1*, indicating oRG identity, while the remaining non-oRG clusters were astrocytes, LIFR-expressing microglia, or newborn neurons according to their mRNA profiles (Figure S6A and S6B). Similarly, most EGFR-panned cells expressed *EGFR*, and these clusters were also enriched for *NES*, *SOX2 and VIM*, consistent with the immunostaining in the fixed brain slices and indicating progenitor identity (Figure S4B, S6A and S6B). Most PDGFRA-panned cells expressed *PDGFRA*, and the major clusters were also enriched for *OLIG1*, *OLIG2*, *NKX2-2* and *SOX10*, indicating OPC identity, while the remaining non-OPC clusters were mainly microglia according to their mRNA profiles (Figure S6A and S6B).

Video frames were captured every 35 minutes over a three-day time window from DIV3 to DIV6, and GFP-labeled progenitors on cultured brain slices were observed to migrate and

divide. Interestingly, most LIFR-panned cells acquired a long radial fiber after transplantation, characteristic of radial glia (Figure S6C). The remaining non-radial cells might represent off-target cells or progeny generated by oRGs during the three days required for cell recovery and virus expression. Both EGFR- and PDGFRA-panned cells exhibited bipolar morphology but did not show any orientation preference (Figure S6C). As expected, the radial cells enriched by LIFR-panning underwent mitotic somal translocation (MST) (Figure 4C and Movie S1), a unique “jump and divide” behavior of oRGs that is not observed in vRGs, neuroepithelial cells, or other known cortical progenitors (Hansen et al., 2010; Noctor et al., 2001; Betizeau et al., 2013; Subramanian et al., 2017). In contrast, PDGFRA-panned cells rounded up in place to divide (Figure 4C). Most EGFR-panned cells also jumped and divided as oRGs did, but the distance of MST was much smaller (Figure 4C and Movie S2). Both daughter cells regrew processes, thereby resembling OPC behavior (Figure 4C). After division, daughter cells of both oRGs and EGFR-panned cells stayed close to each other, while the daughter cells of OPCs rapidly migrated away from each other. Figure 4D and 4E show the quantification of MST distance and daughter cell distance from 30 samples of each type of cell. Both time stamped still images and statistic results indicate that EGFR-expressing cells exhibit their own unique proliferation pattern, but with features resembling a combination of oRG and OPC behavior, consistent with an identity as an intermediate progenitor between oRGs and OPCs. Lineage reconstruction by monocle based on scRNA-seq data of unbiased captured cells (Bhaduri et al., 2020) also supports the developmental trajectory from oRGs to EGFR-expressing IPCs to OPCs (Figure S6D).

We next incubated brain slices with either EGF or EGFR inhibitor Iressa after EGFR-panning, virus labeling, and cell transplantation. When post-stained for NKX2-2 and GFP at DIV7 and compared with DSMO treated control slices, EGF treatment increased while Iressa treatment decreased OPC production from EGFR-panned cells (Figure 4E), indicating an essential role of EGFR-expressing cells in OPC generation.

Transient Amplification of Human OPCs in the Late Second Trimester

We next focused on the proliferative ability of OPCs by studying the time-lapse image data generated above. An average of 20 cells were found to divide within a single visual field, and

42 cells were observed to undergo two rounds of division in the total of twenty-four visual fields. Figure 5A shows an example of an OPC that divided to generate two daughter cells, both of which divided again at similar time points to produce four granddaughter cells (Movie S3). These observations suggest that OPCs undergo frequent repeated symmetric divisions to exponentially increase the progenitor cell pool. This differs from observations of the mouse brain at comparable neonatal ages, where *NG2*-expressing OPCs divide only once in a five-day period to generate two daughter cells that continue to express NG2 for several days before one or both differentiate into oligodendrocytes (Zhu et al, 2011; Hill et al., 2014).

Since OPCs migrate actively in our time-lapse recordings, daughter cells often migrate out of the field of vision, making it difficult to quantitatively analyze the percentage of continuously dividing OPCs by live imaging. Thus, we performed thymidine analog labeling to quantify cell divisions (Figure 5B). OPCs were enriched by PDGFRA-immunopanning and labeled with *CMV-GFP* adeno-virus prior to transplantation into cultured brain slices. Our time-lapse imaging indicated that the time interval between two rounds of division was about 36h. Considering that thymidine is incorporated into cells at S-phase, and G1-phase is usually the longest phase of the cell cycle, we incubated the brain slices with the thymidine analog, chlorodeoxyuridine (CldU), for 12h followed by 24h without thymidine analog, and then another 12h exposure to the thymidine analog, iododeoxyuridine (IdU), followed by 24h without thymidine analog prior to fixation. This was intended to differentially label successive rounds of cell division and to avoid CldU and IdU incorporation into cells during the same S-phase. Three rounds of washing with DPBS after CldU and IdU incubation ensured removal of unincorporated thymidine analog. After fixation we stained the brain slices with OLIG2-antibody to confirm the oligodendrocyte lineage identity of the *GFP*-virus labeled PDGFRA-immunopanned cells (Figure 5B). Quantitative analysis showed that nearly 95% of GFP cells were $OLIG2^+$, indicating a high efficiency of OPC enrichment. Figure 5B is a high magnification image showing an example of a GFP labeled PDGFRA-immunopanned cell that expresses OLIG2 and is co-labeled with both CldU and IdU. Approximately 35% of GFP^+OLIG2^+ cells were either CldU or IdU positive, while 8% of GFP^+OLIG2^+ cells were both CldU and IdU positive, indicating two rounds of cell division after OPC commitment (Figure 5B). Considering that cells were exposed to the thymidine analog for only one third of their cycle, and that the

cycling OPCs were unsynchronized, the proportion of cycling cells should be triple the thymidine analog-labeled number.

Both time-lapse imaging and thymidine analog labeling suggest continuous division of OPCs in the developing human brain. This is consistent with our findings based on staining of fixed brain sections indicating that both bipolar early-OPCs and multipolar late-OPCs are KI67^{+}. These results support the concept that during human cortical development, OPCs undergo a prolonged period of proliferation before differentiation and thus act as transit amplifying cells to greatly increase the progenitor pool through symmetric division. Presumably, the significant increase in OPCs at this stage helps produce the large number of oligodendrocytes needed to myelinate the expanded human cortex.

OPC-enriched *PCDH15* Mediates Daughter Cell Separation and Dispersal after Division

Previous studies and our above time-lapse imaging of LIFR- and EGFR-panned cells have shown that the daughter cells of progenitors usually stay in contact or close to each other long after division (Hansen et al., 2010; Betizeau et al., 2013; Subramanian et al., 2017). However, our time-lapse imaging of PDGFRA-panned cells revealed an unusual behavior of OPC daughter cells following division that differed from the post-mitotic behavior of other progenitors such as RGs and IPCs. Immediately following OPC division, the newly generated daughter cells appeared to repel each other and migrated rapidly in opposite directions (Figure 6C). We reasoned that this behavior might serve to ensure broad distribution of OPCs across the developing cortex.

To explore the mechanism underlying repulsion, we first compared the RNA profiles of dividing OPCs with other dividing cortical progenitors, whose daughters do not repel each other after division (RGs and IPCs). The list of differentially expressed genes included the cell surface molecules *PCDH15* and *DSCAM*, which ranked high among OPC-enriched genes (Figure 7A and 7B). DSCAM belongs to the immunoglobulin superfamily of cell adhesion molecules. It promotes repulsion between neurites and mediates tiling between neurons (Fuerst et al., 2008; Hattori et al., 2008). PCDH15 is a member of the protocadherin superfamily. Although the

function of PCDH15 in OPC development is unknown, other members of the protocadherin family have been reported to mediate dendritic self-avoidance (Lyfebvre et al., 2012).

In order to study the function of PCDH15 and DSCAM in OPCs, we sought to knockdown *PCDH15* or *DSCAM* by shRNA lentivirus. Four shRNA hairpins for *PCDH15* (*PCDH*15-shRNA-A/B/C/D) and *DSCAM* (*DSCAM*-shRNA-A/B/C/D), respectively, were designed and two each were found to down-regulate either *PCDH15* (*PCDH*15-shR-C/D) or *DSCAM* (*DSCAM*-shRNA-A/B) at both mRNA and protein levels in HEK293T and OPCs (Figure S7A and S7B). We performed PDGFRA-immunopanning to enrich human OPCs at GW20-24 and infected them with either *PCDH15*-shRNA-*GFP* or *DSCAM*-shRNA-*GFP* lenti-virus. After three hours of virus incubation we transplanted the virus infected OPCs into cultured cortical slices and performed time-lapse imaging three days later. The scramble-control exhibited similar behavior to that observed in the *CMV-GFP* adeno-virus labeled cells (Figure 5A and Movie S3), namely OPC daughter cells repelled each other and migrated rapidly in opposite directions (Figure 6C and Movie S4). In contrast, the *PCDH15*-shRNA infected daughter cells remained in contact with or close to each other following division, often for many hours (Figure 6C and Movie S5). Quantitative analysis of daughter cell distance from one another showed dramatic increase from 5 to 10 to 15 hours after OPC division in the scramble control, while the separation between daughter cells was much smaller in both *PCDH15*-shRNA-C and -D at the same time point, with no obvious increase between different time points (Figure 6D), indicating significant inhibition of daughter cell dispersion after *PCDH15* knockdown. Statistical analysis of the migration speed before division shows no obvious difference between scramble-control and *PCDH15*-shRNA (Figure 6E), indicating that the inhibition of OPC dispersion is not due to an underlying mobility defect. The *DSCAM*-shRNA infected OPCs repelled each other similarly to control, indicating DSCAM is dispensable for daughter cell repulsion.

To confirm that PCDH15 plays a key role in OPC daughter cell repulsion, we blocked PCDH15 function by antibody incubation instead of shRNA mediated gene knockdown. Again, OPCs were enriched by PDGFRA-immunopanning and labeled with *CMV-GFP* adeno-virus. Two days after cell transplantation we applied PCDH15-antibody to the cultured brain slices and performed live imaging. Since PCDH15 is a membrane-tethered protein, the PCDH15-antibody

that we chose binds to the extracellular domain and would be expected to block protein function. FACS of live HEK293T cells overexpressing protocadherin indicated that PCDH15-antibody had preferential affinity to PCDH15- but not other protocadherin family members (Figure S7C). Adjacent brain slices injected with *GFP* labeled OPCs and exposed to the same concentration of IgG derived from the corresponding animal species served as a control. OPC behavior was normal in the control slices (Figure S7D and Movie S6), while a similar abnormality as in the *PCDH15*-shRNA was observed in the PCDH15-antibody treated brain slices; newly generated OPC sister cells stayed together long after cell division (Figure S7D and Movie S7). Thus, both shRNA knockdown and antibody blocking indicated that PCDH15 is required for daughter cell separation after OPC division, a behavior that might be important for evenly distributing OPCs across the cortex.

Homeostatic Control of OPC Density by PCDH15

As self-avoidance is often closely related to tilling (Hattori et al., 2008), we wondered whether PCDH15 plays a role in OPC tiling, a phenomenon that distributes OPCs in a non-redundant manner to maximize coverage of the surface while minimizing overlap between neighboring OPCs (Hughes et al., 2013). Cultured human cortical slices were incubated with PCDH15 antibody and fixed at DIV7. Staining with O4 and OLIG2 were performed to show the processes and nuclei of the OPCs. In comparison with IgG-control, PCDH15-antibody treated slices showed no significant differences in either process arborization or soma distribution (Figure 7A), indicating PCDH15 may not be involved in OPC tiling. Furthermore, when we analyzed the time-lapse imaging data of PDGFRA-panned cells, we observed no obvious repulsion between two random OPCs when they encounter each other (Movie S8), indicating PCDH15-mediated repulsion might only occur between daughter cells when they separate right after division.

We noticed that many PCDH15-shRNA daughter cells did not re-enter the cell cycle, even long after dividing (>40hr), while the Scramble-control OPCs usually underwent two rounds of division during this same interval. Figure 7B shows one *PCDH15*-shRNA infected OPC sample that divided to generate two daughter cells close to each other. Instead of both daughter cells dividing to generate four granddaughter cells at a second round of division (Figure 5A), only

one daughter cell divided to generate two granddaughter cells close to each other, while the other daughter cell remained quiescent (Movie S9). This suggests that failure of dispersion of daughter cells might inhibit further division, potentially helping to achieve homeostatic control of local OPC density. We sought to quantify whether knockdown of PCDH15 affects OPC proliferation. We fixed cultured human cortical slices treated with PCDH15-antibody at DIV7 and post-stained them with NKX2-2 and KI67. There was no significant difference in the density of NKX2-2^{+} cells between IgG-control and PCDH15-antibody blocking, while both the number and percentage of NKX2-2^{+}KI67^{+} cells were decreased dramatically after incubation with PCDH15-antibody compared with IgG-control. Both time-lapse imaging and antibody blocking experiments support the idea that PCDH15-mediated daughter cell separation and dispersion prevent local OPC accumulation and facilitate OPC proliferation.

DISCUSSION

Due to restricted access to human tissue samples and a limited capacity for experimental manipulation, most of our knowledge about gliogenesis has been obtained from studies in animal models, primarily rodents, while relatively little is known about human oligodendrogenesis. During evolution, the human neocortex enlarged dramatically with considerable expansion of not only grey matter, but also white matter. The evolutionary expansion of grey matter has been attributed to a prolonged gestational period as well as the presence of novel neural stem cell populations and intermediate progenitor cells that greatly increase the neuronal output of cortical germinal niches. However, little is known about the mechanisms underlying white matter expansion and how oligodendrocyte production is regulated to meet the increased demands for myelination. Developmental features of oligodendrocyte precursor cells observed in animal models might not apply to human brain development, particularly given the large structural and volume differences between human and rodent cortex. By combining scRNA-seq analysis, *in vivo* immunohistochemistry, *ex vivo* brain slice culture, and time-lapse imaging, we map the lineage trajectory of oligodendrogenesis in the developing human cortex and identify a novel type of intermediate progenitor cells (EGFR-expressing Pre-OPCs) in the OSVZ that generate OPCs. We also discover that oRG cells are an additional source of cortical OPCs in the developing human brain that has not been observed in rodents, and uncover an enhanced proliferative ability of

embryonic OPCs that helps to produce the large number of oligodendrocytes associated with human cortical expansion. We further demonstrate repulsive behavior between OPC daughter cells, mediated by an OPC-specific protocadherin family member, *PCDH15*, which promotes dispersal of OPCs and facilitates OPC proliferation. These findings extend our comprehension of human cortical expansion and human oligodendrogenesis.

The Role of oRGs in Human Cortical Oligodendrogenesis

During peak periods of neurogenesis in human cortical development (GW13-19), oRGs populate the OSVZ and produce EOMES-expressing transit-amplifying IPCs that ultimately generate neurons. The abundance of oRGs in primates contributes to the production of large numbers of neurons and provides a secondary radial glia scaffold to support neuronal migration (Lui et al., 2011; Taverna et al., 2014; Fernandez et al., 2016; Gertz, et al., 2015). However, direct evidence for a possible role of oRGs in gliogenesis is lacking (Rowitch and Kriegstein, 2010). A recent study of the developing macaque suggested that oRGs support oligodendrogenesis, but lacked functional validation, highlighting the need for experimental studies to determine the identity and role of oligodendrocyte progenitors in the developing primate brain (Rash et al., 2019). Here, by combining scRNA-seq analysis with immunohistochemistry and primary cell culture, we find evidence for oRG-derived OPC generation in the cerebral cortex. Our study highlights the important role of oRGs for both neurogenesis and gliogenesis. It will be interesting to further compare early neurogenic oRGs with late oligodendrogenic oRGs, and study the mechanisms underlying the temporal switch from neurogenesis to oligodendrogenesis.

EGFR-expressing Intermediate Progenitors and Oligodendrogenesis

EGFR is widely recognized for its importance in cancer, where excessive activation of EGFR signaling often leads to hyper-proliferation of tumor cells (da Cunha Santos et al., 2011; Eskilsson et al., 2018). Here, at the onset of gliogenesis, we find that large numbers of EGFR expressing progenitors occupy germinal zones of the embryonic human cortex and support OPC production. Both lineage reconstruction and differentiation assays indicate that oRGs do not generate OPCs directly, instead EGFR-expressing cells act as intermediate progenitors for oligodendrogenesis. The existence of proliferative Pre-OPCs lying between the oRGs and

OPCs in the lineage trajectory may serve to increase the rounds of division and enlarge the progenitor pool. The responsiveness of Pre-OPCs to EGF suggests a tight regulation of OPC production by EGF secreted in the progenitor cell niche of the developing cortex. Interestingly, we find that a subset of oRGs express *EGF* mRNA in our scRNA-seq database. This suggests a possible mechanism for coordination between neurogenesis and oligodendrogenesis, which could serve to match the increase in neuron production to the requirement of more oligodendrocytes for axon myelination. Alternatively, it might represent a positive feed forward mechanism to facilitate OPC production.

Pre-OPCs in Mouse and Human Brain

Co-expression of NPC genes with early OPC markers has helped to illuminate OPC origins. A form of Pre-OPCs has been identified in the mouse forebrain by scRNA-seq of PDGFRA-GFP^{+} cells (Marques et al., 2018). The Pre-OPCs, present at E13.5 but nearly absent at E17.5, express markers of both NPCs and OPCs and represent a transitional stage from NPCs to OPCs. Bulk tissue sequencing indicates that transcription factors involved in ganglionic eminence patterning (*Otx2*, *Nkx2-1*, and *Arx*) are highly expressed in these mouse Pre-OPCs (Marques et al., 2018), consistent with the concept that ventral-derived NPCs are the main source of mouse forebrain OPCs at early embryonic stages (Kessaris et al., 2006). Similarly, scRNA-seq of cells from the ventral midbrain of E13.5 mouse and PCW 10-11 (GW8-13) human have identified radial glia-like cell types that express OPC markers, representing a transitional stage from basal plate radial glia to OPCs (La Manno, et al. 2016). In contrast, our Pre-OPCs are identified at much later ages during GW20-24 and have not been described in mice at comparable ages (postnatal days) (Marques et al., 2018). They co-express some of oRG markers, exhibit hybrid MST behavior and are mainly located in the OSVZ, indicating a prolonged period of NPC to OPC transition in the developing human cortex and a source of oRG-derived OPCs absent in mouse. Our findings combined with mouse and early stage human data summarized above support the notion that diverse NPCs and Pre-OPCs converge into similar transcriptional OPC states (Marques et al., 2018).

Progenitor Diversity in the OSVZ

During evolution, primates developed an enlarged cortical germinal zone, the OSVZ, which is lacking in most rodents. Previous studies have highlighted the critical role of the OSVZ as a site for neuron production in large-brain mammals (Hansen et al., 2010; Fietz et al., 2010; Betizeau et al., 2013; Nonako-Kinoshita et al., 2013). Here we find large numbers of dividing progenitor cells that support OPC production, including oRGs, Pre-OPCs, and OPCs, in the human OSVZ and neighboring IZ at the onset of gliogenesis. The OSVZ and IZ together span more than half of the total cortical thickness at the end of the second trimester. Such a relatively large area, populated by a high density of $KI67^+$ progenitors, facilitates production of large numbers of neurons and glia. At stages of peak neurogenesis (GW13-19) the OSVZ contains two major types of progenitors, oRGs and neurogenic IPCs, while at later stages the progenitor cell types of the OSVZ appear to be more diverse. At GW20-24, we identify at least four types of progenitors in the OSVZ, including $GFAP^+pS6^+SOX2^+$ oRGs, $EOMES^+SOX2^-$ IPCs, $EGFR^+SOX2^+OLIG2^+$ Pre-OPCs, and $EGFR^-PDGFRA^+OLIG2^+$ OPCs. Considering that astrocyte production also occurs at this stage, and that both oligodendrogenesis and astrogenesis continue through the third trimester, the progenitor cell types are likely to be even more diverse than outlined above. It will be interesting to study progenitor cell diversity at these later stages and learn how progenitors may interact to coordinate neurogenesis and gliogenesis.

Symmetric Division and Transit Amplification

OPCs maintain the ability to self-renew and continuously generate oligodendrocytes throughout life (Kang et al., 2010; Young et al., 2013). But unlike embryonic OPCs, most OPCs in the adult brain are quiescent under normal conditions (Yeung et al., 2014). Here we observe that OPCs in the developing human cortex act as transit amplifying cells, continuously proliferating through symmetric division to exponentially increase the oligodendrocyte progenitor pool. As a result, in a prolonged period spanning at least five weeks (GW20-24), large quantities of OPCs can be generated, producing oligodendrocytes sufficient to populate the large area of expanded white matter. Interestingly, nearly all $PDGFRA^+OLIG2^+$ OPCs at this stage are $SOX2^+$, consistent with previous reports that SOX2 maintains OPCs in a proliferative state and inhibits differentiation (Zhao et al., 2015). OPCs may also serve as a cell of origin for glioblastoma (Persson et al., 2010; Liu et al., 2011; Zong et al., 2015; Weng et al.,

2019). Considering that OPC-like tumor cells are hyper-proliferative, they may be closer to embryonic human OPCs than more mature adult OPCs. Here we provide gene signatures for embryonic human OPCs, and comparisons of the mRNA-profiles of adult human OPCs, embryonic human OPCs, and OPC-like tumor cells may provide an opportunity to discover key molecules that may be essential for hyper-proliferation and could serve as candidate targets for tumor therapy.

Cell Repulsion and Homeostatic Control of OPC Density

In the adult mouse brain, OPCs occupy mutually exclusive territories through a balance between proliferation and self-repulsion, although the molecular mechanisms are unknown (Hughes et al., 2013). In the embryonic human cortex, we observe a self-avoidance behavior between daughter cells following OPC division. This behavior is very unique compared with the phenotype observed in other dividing cells of the developing cortex, including RGs or IPCs, where daughter cells stay in contact long after division (Noctor et al., 2001; Hansen et al., 2010; Betizeau et al., 2013). This is particularly notable when RGs divide asymmetrically to self-renew and generate a neuron, which remains in contact with the parent RG fiber as it migrates. Consecutive divisions of individual RGs and their IPC daughter cells produce a clone of sister cells that remain in contact and eventually form a columnar array of clustered neocortical neurons (Noctor et al., 2001; Yu et al., 2009). In contrast, when OPCs in our study divide symmetrically, the two daughter OPCs strongly repel each other and migrate in opposite directions. This behavior likely serves to avoid local accumulation and ensure broad distribution of OPCs. We find that the mechanism of repulsion involves the protocadherin superfamily member PCDH15 that is selectively enriched in OPCs. According to our differential expression data, DSCAM is also enriched in OPCs, but our functional assays indicate it is not involved in daughter cell repulsion, highlighting the specificity of PCDH15 for OPC dispersion. Furthermore, we observe that failure of daughter cell separation impairs the ability of daughter cells to engage in subsequent divisions, reflecting a cellular mechanism underlying homeostatic control of OPC density during development and highlighting the importance OPC dispersion on OPC proliferation and white matter expansion.

Unique Gene Expression Profile of OPCs

PCDH15 is not only a gene differentially expressed between dividing OPCs and RGs or IPCs, but also serves as a marker gene for OPCs. Because our database was composed of most cell types present in the developing human cerebral cortex, including RGs, IPCs, neurons, astrocytes, and microglia, our gene expression database afforded an opportunity to discover new marker genes for OPCs. Differential gene expression analysis highlighted several additional cell type-specific candidate genes, such as *LHFPL3*, *B3GNT7*, *LUZP2*, and *SCN1A* (Figure S8A). Future work elucidating the function of these genes in OPC biology may provide insight into human oligodendrocyte development.

OPCs and Cerebral Cortical Malformation

High throughput sequencing has uncovered a number of gene mutations related to cortical malformations including microcephaly, lissencephaly, and polymicrogyria (Walsh, 1999; Hu et al., 2014). Although a majority of the gene mutations in patients are germ line mutations, most studies of the molecular and cellular mechanisms have focused on the neuronal lineage, while abnormalities in glia have generally not been considered. Our scRNA-seq dataset shows that many genes related to brain malformation are also enriched in OPCs. For example, the microcephaly related genes *ASPM*, *STIL*, *CEP135*, *CDK6*, *RBBP8*, *CEP152* and *CENPJ* are all highly expressed in neuronal progenitors including dividing RGs and IPCs, but they are also highly expressed in dividing OPCs (Figure S8B), suggesting that disease-causing mutations in these genes might also directly interfere with the production of oligodendrocytes, and thus contribute to microcephaly. Additionally, our dataset indicates that many polymicrogyria related genes are expressed broadly in both neural progenitors and OPCs, and many of the genes, such as *GPR56*, *ATP6V0A2*, *GPSM2*, *NDE1*, *RAB18*, *CCND2*, *PTEN*, *DYNC1H1*, *KIF5C*, *TUBA1A*, *TUBB2A*, *TUBB2B*, *BICD2*, *DDX3X*, *EZH2* and *OFD1*, show equal or even higher expression levels in OPCs compared with other cell types (Figure S8C). This strongly suggests that an abnormality in OPCs might contribute to polymicrogyria. Together, these cell-type selective gene expression patterns can inform future analysis of genetic variants associated with neurodevelopmental diseases.

ACKNOWLEDGEMENTS

We thank Hiroko Nobuta, Manideep Chavali, and Shawn Sorrells for providing resources, suggestions and technical assistance. Donated tissue samples were obtained in strict compliance with institutional guidelines and ethical oversight. This research was supported by NIH awards P01NS083513 (to D.H.R. and A.R.K.), U01 MH105989 and R01NS075998 (to A.R.K).

AUTHOR CONTRIBUTIONS

A.R.K., W.H., A.A.B., and D.H.R. conceived and supervised the project. W.H. designed and performed all the functional experiments. A.B. and D.V. performed bioinformatics analysis. S.W. collected tissue samples and made the frozen sections for immunohistochemistry. L.W. performed shRNA efficiency test and FACS based antibody specificity test. C.A.R. initiated this project. W.H., A.R.K., and D.H.R. wrote the manuscript with the input from all authors.

DECLARATION OF INTERESTS

A.R.K. is a co-founder and board member of Neurona Therapeutics.

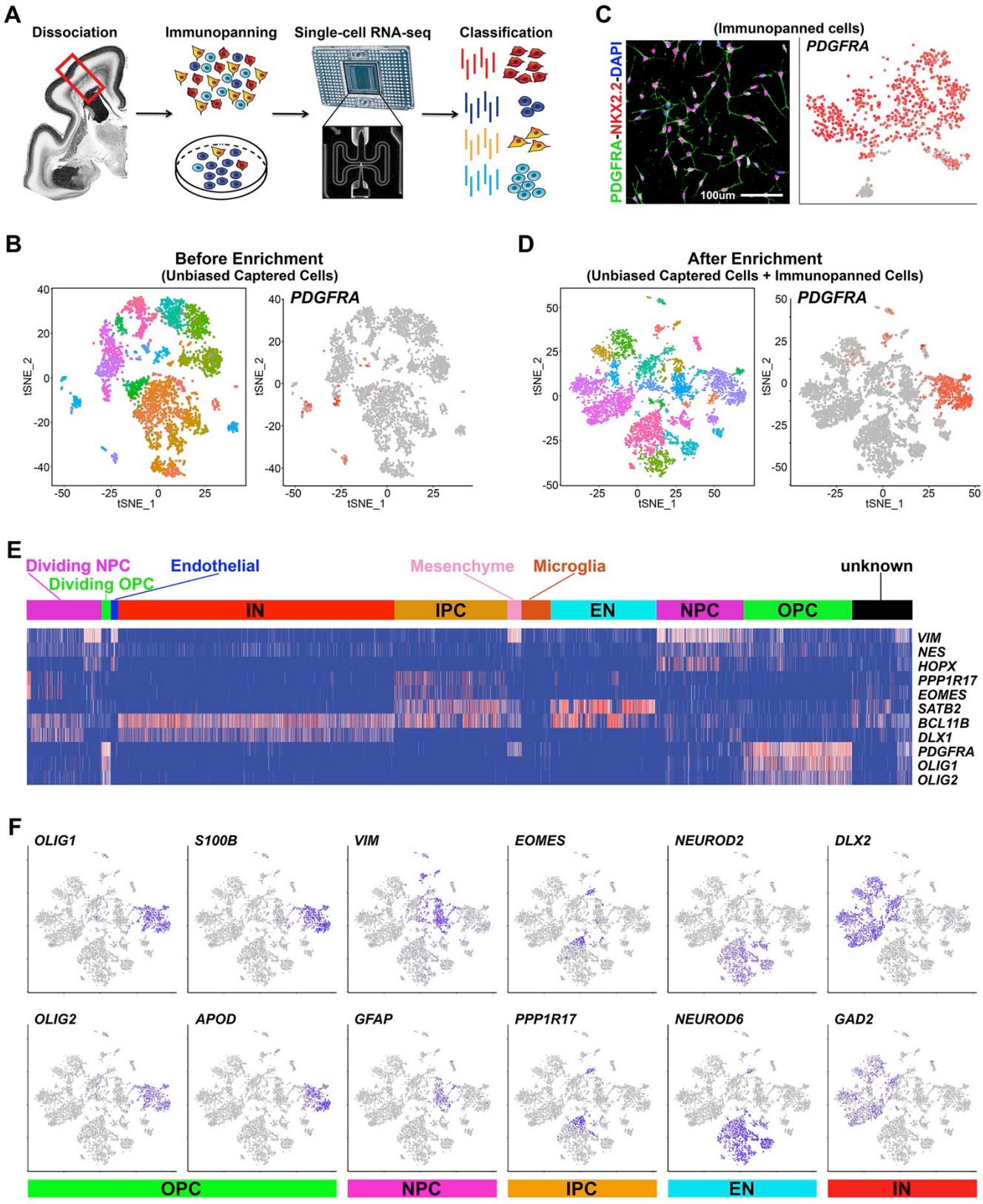
A
Dissociation
Immunopanning
Single-cell RNA-seq
Classification
C
(Immunopanned cells)
PDGFRA-NKX2.2-DAPI
100um
PDGFRA
B
Before Enrichment
(Unbiased Captered Cells)
PDGFRA
tSNE_1
tSNE_2
D
After Enrichment
(Unbiased Captered Cells + Immunopanned Cells)
PDGFRA
tSNE_1
tSNE_2
E
Dividing NPC
Dividing OPC
Endothelial
Mesenchyme
Microglia
unknown
IN
IPC
EN
NPC
OPC
VIM
NES
HOPX
PPP1R17
EOMES
SATB2
BCL11B
DLX1
PDGFRA
OLIG1
OLIG2
F
OLIG1
S100B
VIM
EOMES
NEUROD2
DLX2
OLIG2
APOD
GFAP
PPP1R17
NEUROD6
GAD2
OPC
NPC
IPC
EN
IN

Figure 1. Single-cell RNA-sequencing of OPCs from the Developing Human Cortex.
(A) Schematic of the workflow. Developing human cortex was dissociated and OPCs enriched by PDGFRA-immunopanning. Single-cells were isolated using the Fluidigim C1 microfluidic chip system, and pair-end single-cell RNA-sequencing performed. Clustering was used to annotate cell types according to RNA profiles.
(B) Scatterplot by tSNE (left) and feature plot of *PDGFRA*-mRNA expression (right) from Nowakowski et al., 2017. Single-cell RNA-sequencing performed on forty-eight individuals mainly at GW14-24 from primary dissociated cortex without enrichment resulted in capture of few OPCs (*PDGFRA*-expressing).
(C) Validation of the immunopanning strategy. Most DAPI-stained cells were $PDGFRA^{+}NKX2\text{-}2^{+}$, while more than 90% of sequenced cells expressed *PDGFRA* mRNA, indicating high efficiency OPC enrichment.
(D) Scatterplot by tSNE (left) and feature plot of *PDGFRA*-mRNA expression (right) of data generated in this study from nine individuals at GW20-24 combined with Nowakowski et al., 2017. A total of 980 OPCs were identified and intermixed with those captured without enrichment (B).
(E) Heatmap showing cluster annotations and marker gene expression.
(F) Feature plots of marker genes. OPCs are segregated from neural progenitor cells (NPC) and intermediate progenitor cells (IPC), and are distinct from excitatory (EN) and inhibitory (IN) neurons.

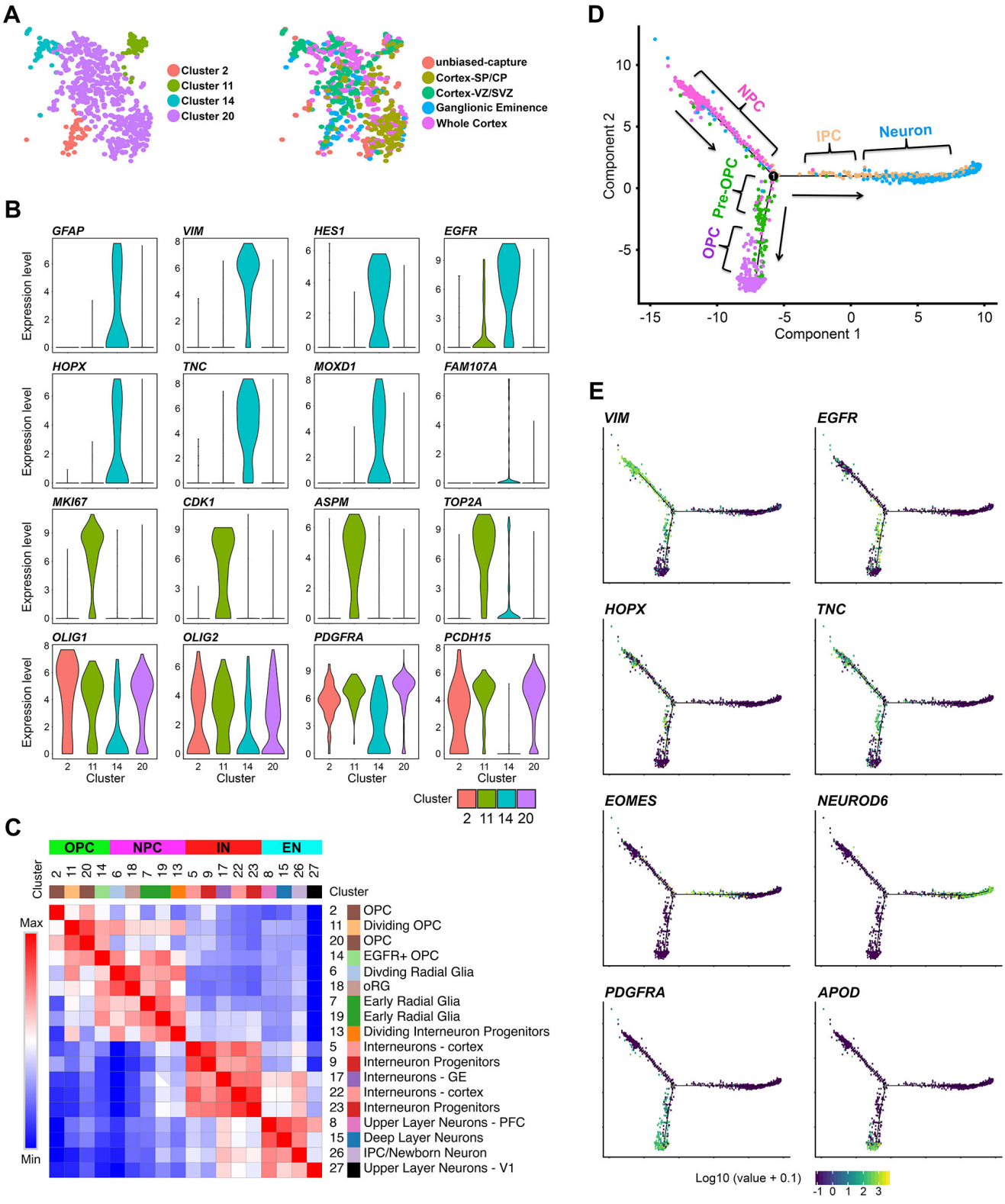
A
Cluster 2
Cluster 11
Cluster 14
Cluster 20
unbiased-capture
Cortex-SP/CP
Cortex-VZ/SVZ
Ganglionic Eminence
Whole Cortex
B
GFAP
VIM
HES1
EGFR
HOPX
TNC
MOXD1
FAM107A
MKI67
CDK1
ASPM
TOP2A
OLIG1
OLIG2
PDGFRA
PCDH15
Expression level
Cluster
2 11 14 20
C
OPC
NPC
IN
EN
Cluster
Max
Min
2 OPC
11 Dividing OPC
20 OPC
14 EGFR+ OPC
6 Divding Radial Glia
18 oRG
7 Early Radial Glia
19 Early Radial Glia
13 Dividing Interneuron Progenitors
5 Interneurons - cortex
9 Interneuron Progenitors
17 Interneurons - GE
22 Interneurons - cortex
23 Interneuron Progenitors
8 Upper Layer Neurons - PFC
15 Deep Layer Neurons
26 IPC/Newborn Neuron
27 Upper Layer Neurons - V1
D
NPC
IPC
Neuron
Pre-OPC
OPC
Component 1
Component 2
E
VIM
EGFR
HOPX
TNC
EOMES
NEUROD6
PDGFRA
APOD
Log10 (value + 0.1)

Figure 2. Characterization of OPC Clusters from Single-cell RNA-sequencing.
(A) Enlarged tSNE plot from Figure 1D focusing on the OPC clusters. Clusters are shown on the left, and metadata annotation of tissue source is represented on the right.
(B) Violin plots of differentially expressed genes in OPC clusters. Marker genes for NPCs and oRGs are enriched in cluster 14 and cell cycling genes are enriched in cluster 11. Pan-OPC marker genes are expressed in all OPC clusters, but are relatively low in cluster 14.
(C) Similarity matrix of OPC, NPC, and neuronal clusters. OPCs are segregated, but cluster 14 resembles NPC.
(D) Trajectory analysis of progenitor and OPC cell types using Monocle. Broad cell types are shown rather than individual clusters.
(E) Feature plots of marker genes for NPCs, IPCs, neurons and OPCs indicating lineage progression. Neuronal and OPC lineages are distinct, but both emerge from NPCs.

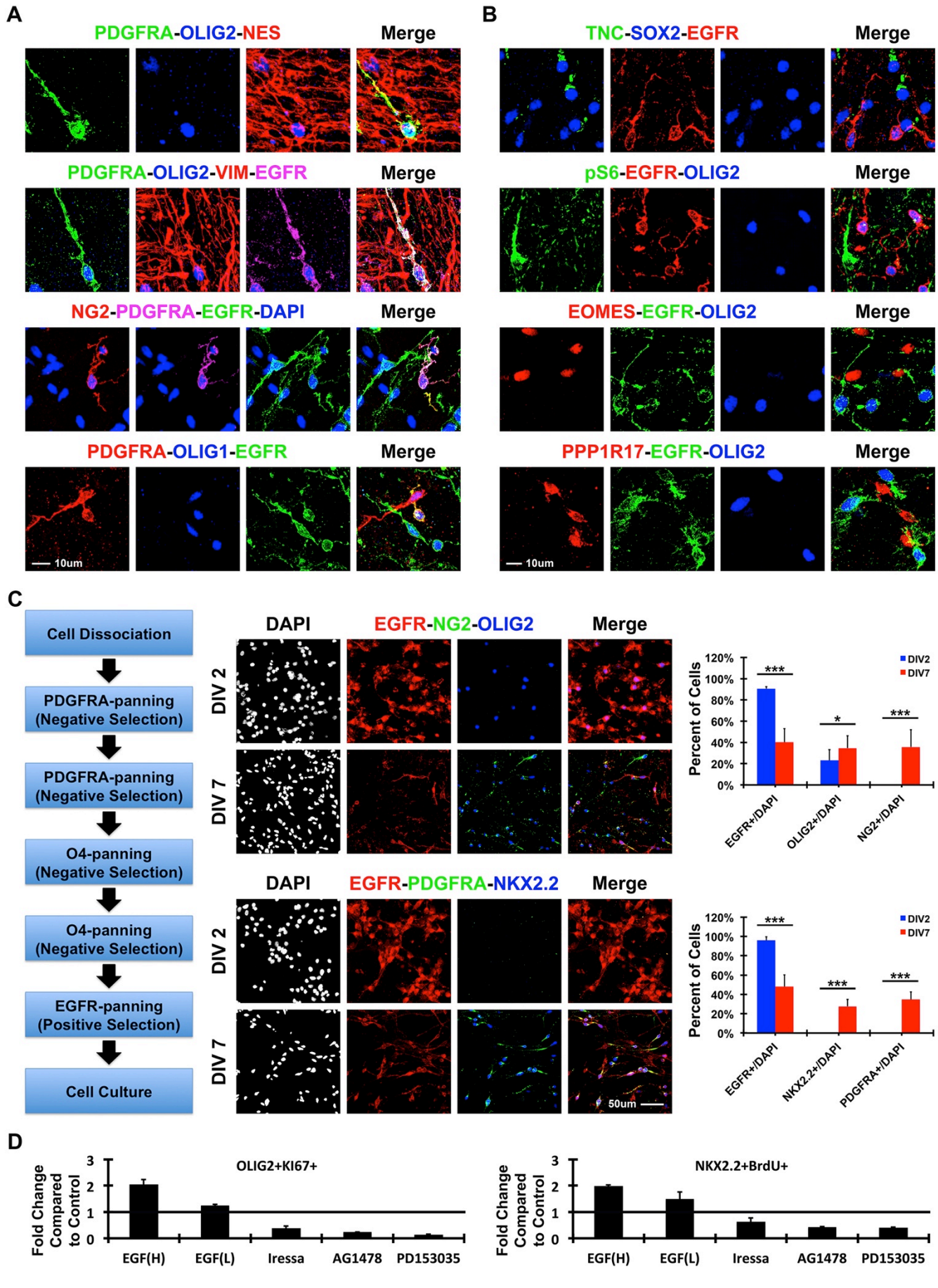
A
PDGFRA-OLIG2-NES
Merge
PDGFRA-OLIG2-VIM-EGFR
Merge
NG2-PDGFRA-EGFR-DAPI
Merge
PDGFRA-OLIG1-EGFR
Merge
10um
B
TNC-SOX2-EGFR
Merge
pS6-EGFR-OLIG2
Merge
EOMES-EGFR-OLIG2
Merge
PPP1R17-EGFR-OLIG2
Merge
10um
C
Cell Dissociation
PDGFRA-panning (Negative Selection)
PDGFRA-panning (Negative Selection)
O4-panning (Negative Selection)
O4-panning (Negative Selection)
EGFR-panning (Positive Selection)
Cell Culture
DAPI
EGFR-NG2-OLIG2
Merge
DIV 2
DIV 7
Percent of Cells
DIV2
DIV7
EGFR+/DAPI
OLIG2+/DAPI
NG2+/DAPI
DAPI
EGFR-PDGFRA-NKX2.2
Merge
DIV 2
DIV 7
50um
Percent of Cells
DIV2
DIV7
EGFR+/DAPI
NKX2.2+/DAPI
PDGFRA+/DAPI
D
OLIG2+KI67+
Fold Change Compared to Control
EGF(H)
EGF(L)
Iressa
AG1478
PD153035
NKX2.2+BrdU+
Fold Change Compared to Control
EGF(H)
EGF(L)
Iressa
AG1478
PD153035

Figure 3. EGFR-positive Progenitors Generate OPCs in the Developing Human Cortex.
(A) Characterization of Pre-OPCs that co-express NPC and OPC markers. Images are from human OSVZ at GW20-24 (n=12).
(B) Characterization of EGFR-expressing progenitors by oRG or IPC marker co-staining. Images are from human OSVZ at GW20-24 (n=12).
(C) Outline of immunopanning workflow (left). PDGFRA and O4 were used to deplete OPCs, and EGFR positive selection enriched for progenitors. Images of marker staining at DIV2 and DIV7 showing lineage progression (middle). Quantification of cell proportions (right). Mean±SD (n=5). (***, $p<0.001$; **, $p<0.01$; *, $p<0.05$; N.S., $p>0.05$.)
(D) Quantification of dividing OPCs inn cultured human brain slices after pharmacologically activating [EGF(High) and EGF(Low)] or inhibiting (Iressa, AG1478, and PD153035) EGFR. Mean±SD (n=6).
See also Figure S1 to S5.

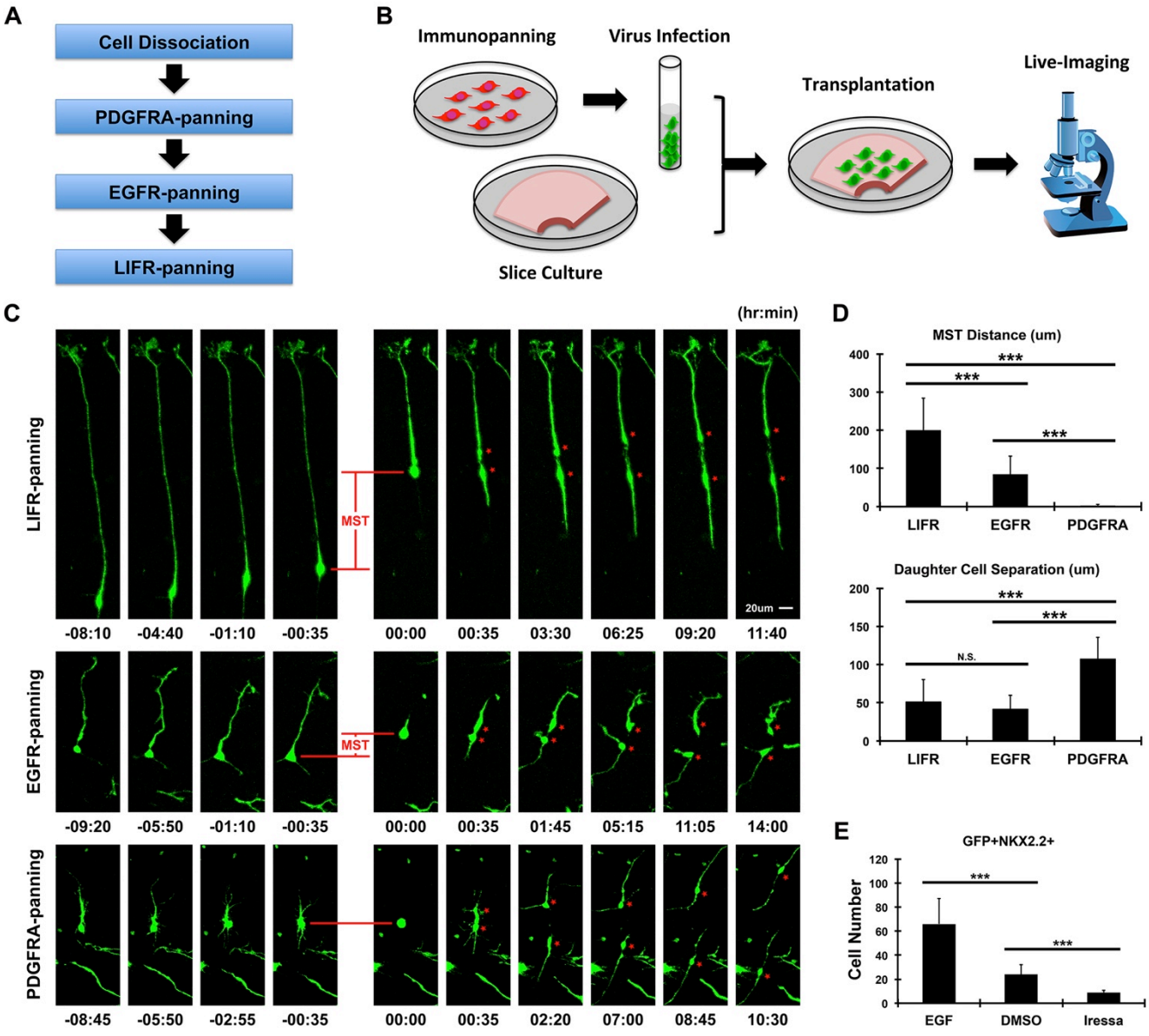
A
Cell Dissociation
PDGFRA-panning
EGFR-panning
LIFR-panning
B
Immunopanning
Virus Infection
Transplantation
Live-Imaging
Slice Culture
C
(hr:min)
LIFR-panning
MST
20um
-08:10
-04:40
-01:10
-00:35
00:00
00:35
03:30
06:25
09:20
11:40
EGFR-panning
MST
-09:20
-05:50
-01:10
-00:35
00:00
00:35
01:45
05:15
11:05
14:00
PDGFRA-panning
-08:45
-05:50
-02:55
-00:35
00:00
00:35
02:20
07:00
08:45
10:30
D
MST Distance (um)
400
300
200
100
0
***
***
***
LIFR
EGFR
PDGFRA
Daughter Cell Separation (um)
200
150
100
50
0
***
***
N.S.
LIFR
EGFR
PDGFRA
E
GFP+NKX2.2+
Cell Number
120
100
80
60
40
20
0
***
***
EGF
DMSO
Iressa

Figure 4. Characterization of EGFR-expressing Progenitors in the Developing Human Cortex.

(A) Outline of immunopanning workflow. Different types of progenitors in the OSVZ were positively selected with PDGFRA-, EGFR- and LIFR-antibody by sequential immunopanning.

(B) Schematic of the experimental strategy. Progenitors were enriched by immunopanning, infected with GFP adeno-virus, injected into cultured cortical slices, and observed for time-lapse imaging.

(C) Time stamped still images of dividing progenitors enriched by LIFR-, EGFR-, or PDGFRA-panning. Representative cells from cultured cortical slices at GW20-24 (n=30).

(D) Quantification of MST distance during division and daughter cell separation of different progenitors at 6 hours after division. Mean±SD (n=30). (***, $p<0.001$; N.S., $p>0.05$.)

(E) Quantification of OPCs from EGFR-panned cells in cultured human brain slices after pharmacologically activating (EGF) or inhibiting (Iressa) EGFR. Mean±SD (n=6). (***, $p<0.001$.)

See also Figure S6 and Movie S1-S2.

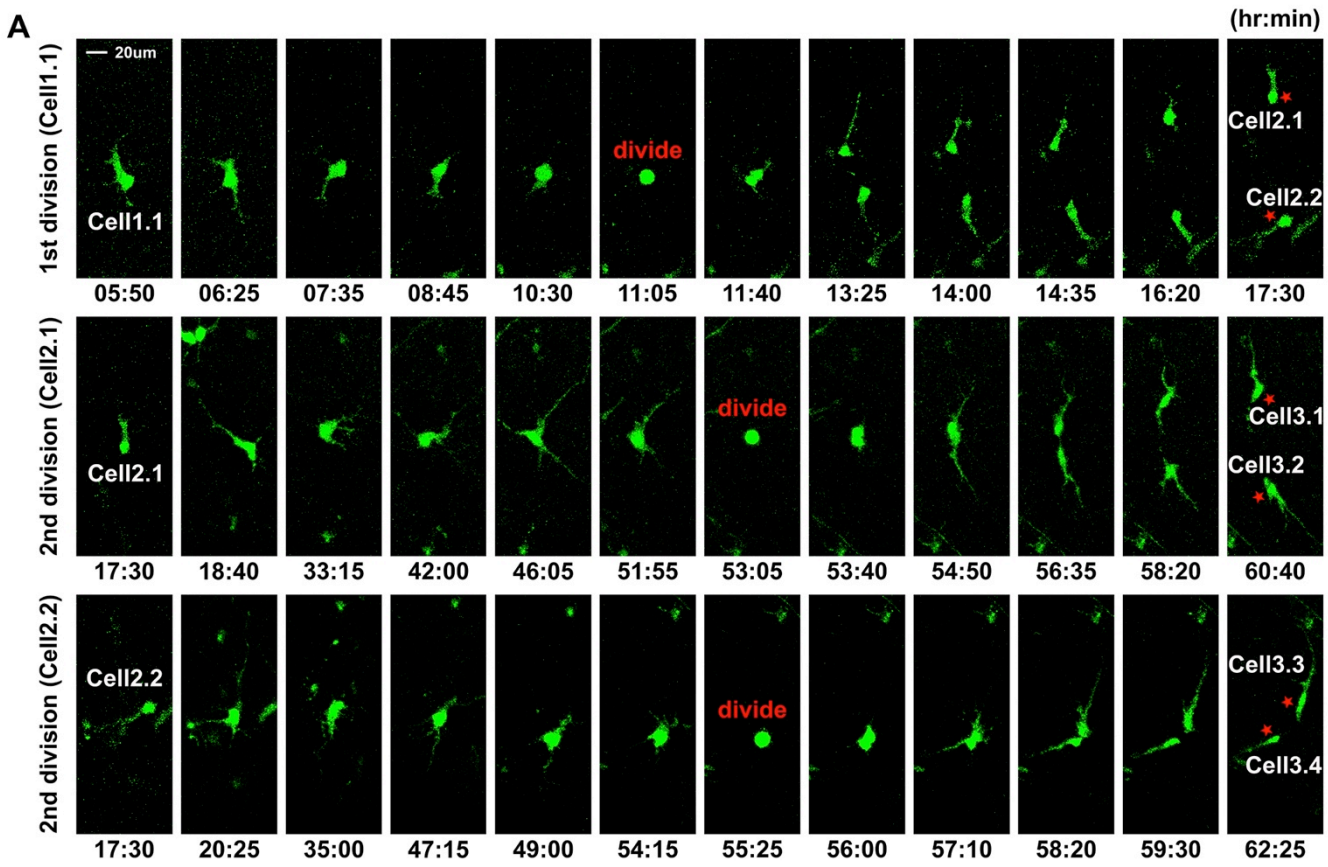
A
(hr:min)
20um
1st division (Cell1.1)
Cell1.1
divide
Cell2.1
Cell2.2
05:50
06:25
07:35
08:45
10:30
11:05
11:40
13:25
14:00
14:35
16:20
17:30
2nd division (Cell2.1)
Cell2.1
divide
Cell3.1
Cell3.2
17:30
18:40
33:15
42:00
46:05
51:55
53:05
53:40
54:50
56:35
58:20
60:40
2nd division (Cell2.2)
Cell2.2
divide
Cell3.3
Cell3.4
17:30
20:25
35:00
47:15
49:00
54:15
55:25
56:00
57:10
58:20
59:30
62:25

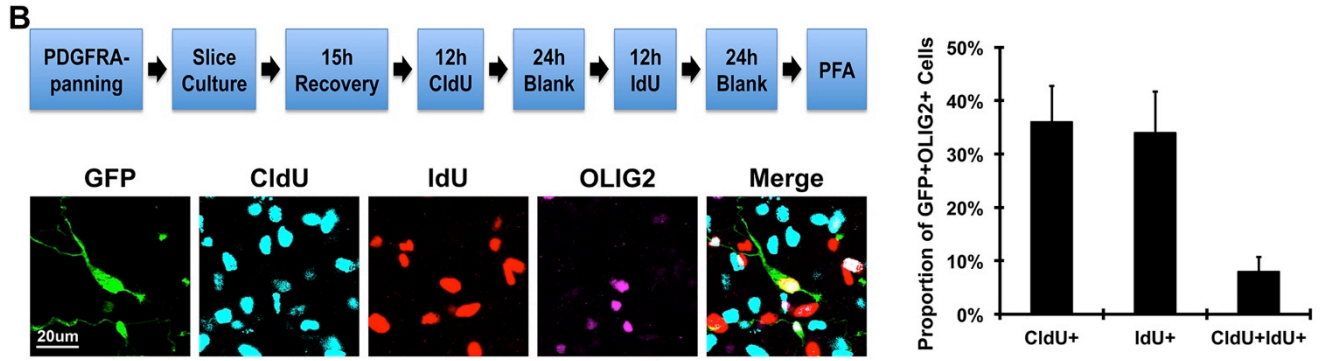
B
PDGFRA-panning
Slice Culture
15h Recovery
12h CldU
24h Blank
12h IdU
24h Blank
PFA
GFP
CldU
IdU
OLIG2
Merge
20um
Proportion of GFP+OLIG2+ Cells
50%
40%
30%
20%
10%
0%
CldU+
IdU+
CldU+IdU+

Figure 5. Characterization of Division Properties of Human Embryonic OPCs.
(A) Time stamped still images of dividing OPCs. Two rounds of continuous division were observed and four granddaughter cells were generated. Representative cell from a cultured cortical slice at GW22 (n=20).
(B) Workflow to explore OPC division quantitatively (top left). OPCs were enriched with PDGFRA-immunopanning, and infected with GFP adenovirus before transplantation and thymidine analog labeling. Representative images from cultured cortical slices at GW20-24 show a GFP-positive immunopanned cell co-labeled with CldU and IdU, and expressing OLIG2 (bottom left) (n=20). Quantification of the proportion of $GFP^{+}OLIG2^{+}$ cells that express either CldU or IdU or both. Mean±SD (right). (n=10)
See also Movie S3.

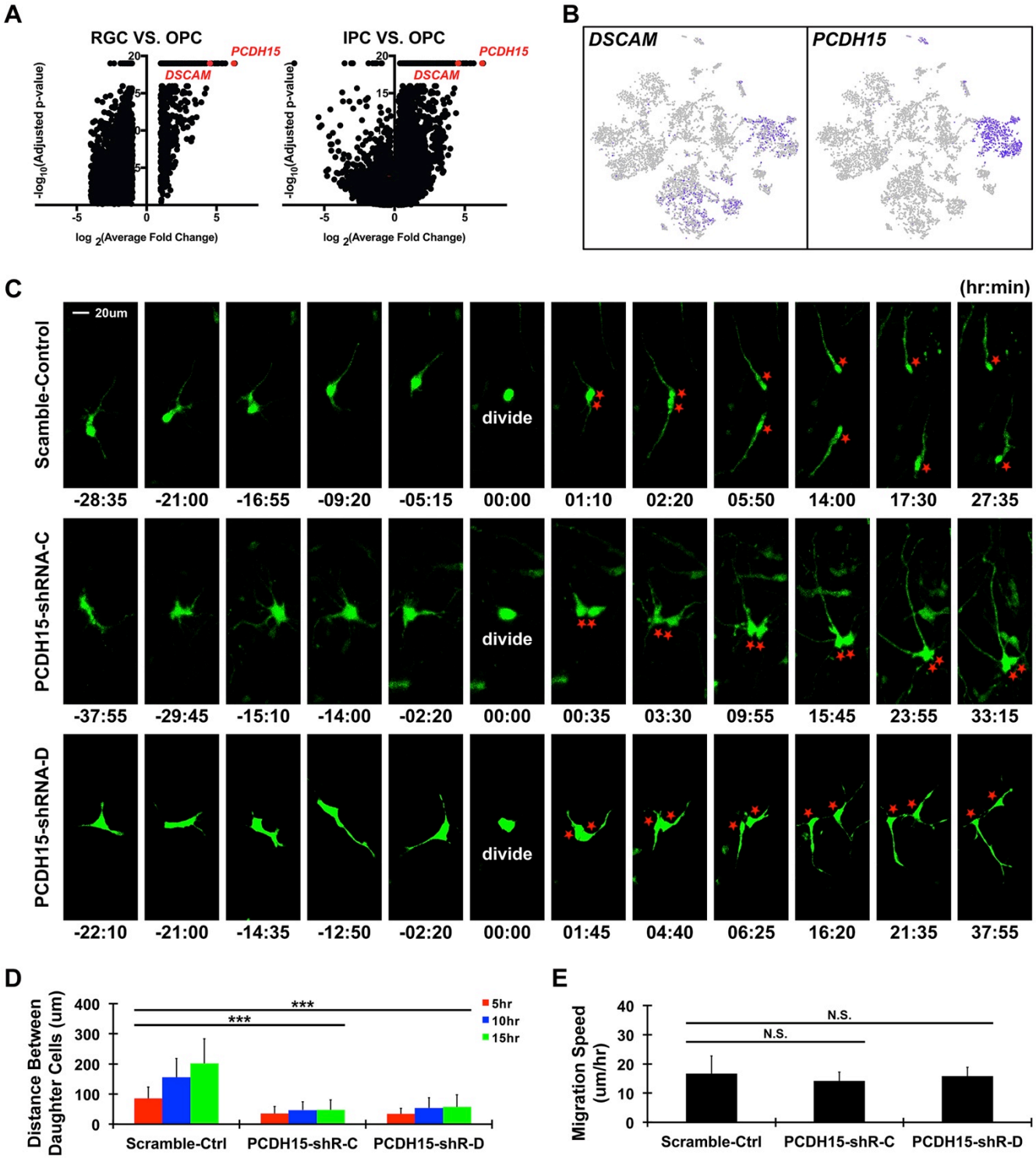
A
RGC VS. OPC
IPC VS. OPC
PCDH15
DSCAM
-log10(Adjusted p-value)
log 2(Average Fold Change)
B
DSCAM
PCDH15
C
(hr:min)
20um
Scramble-Control
PCDH15-shRNA-C
PCDH15-shRNA-D
divide
-28:35
-21:00
-16:55
-09:20
-05:15
00:00
01:10
02:20
05:50
14:00
17:30
27:35
-37:55
-29:45
-15:10
-14:00
-02:20
00:00
00:35
03:30
09:55
15:45
23:55
33:15
-22:10
-21:00
-14:35
-12:50
-02:20
00:00
01:45
04:40
06:25
16:20
21:35
37:55
D
Distance Between Daughter Cells (um)
***
***
5hr
10hr
15hr
Scramble-Ctrl
PCDH15-shR-C
PCDH15-shR-D
E
Migration Speed (um/hr)
N.S.
N.S.
Scramble-Ctrl
PCDH15-shR-C
PCDH15-shR-D

Figure 6. PCDH15 Mediates Daughter Cell Repulsion after OPC Division.
(A) Volcano plots show differentially expressed genes between dividing OPCs and dividing RGs (left) or dividing IPCs (right). Two of the most highly differentially expressed genes are *DSCAM* and *PCDH15*.
(B) Feature plots of *DSCAM* (left) shows expression in excitatory neurons and OPCs, while *PCDH15* is specific to OPCs.
(C) Time stamped still images of dividing OPCs treated with either scramble-shRNA control lentiviruses or *PCDH15*-shRNA lentiviruses to interfere with PCDH15 function. The control division resulted in repulsion between daughter cells. With PCDH15 interference, the daughter cells remained close to each other. Representative cells are from cultured cortical slices at GW20-24 (n=30).
(D) Quantification of daughter cell distance after division. Mean±SD (n=30). (***, $p<0.001$.)
(E) Quantification of migration speed before division. Mean±SD (n=30). (N.S., $p>0.05$.)
See also Figure S7 and Movie S4-S7.

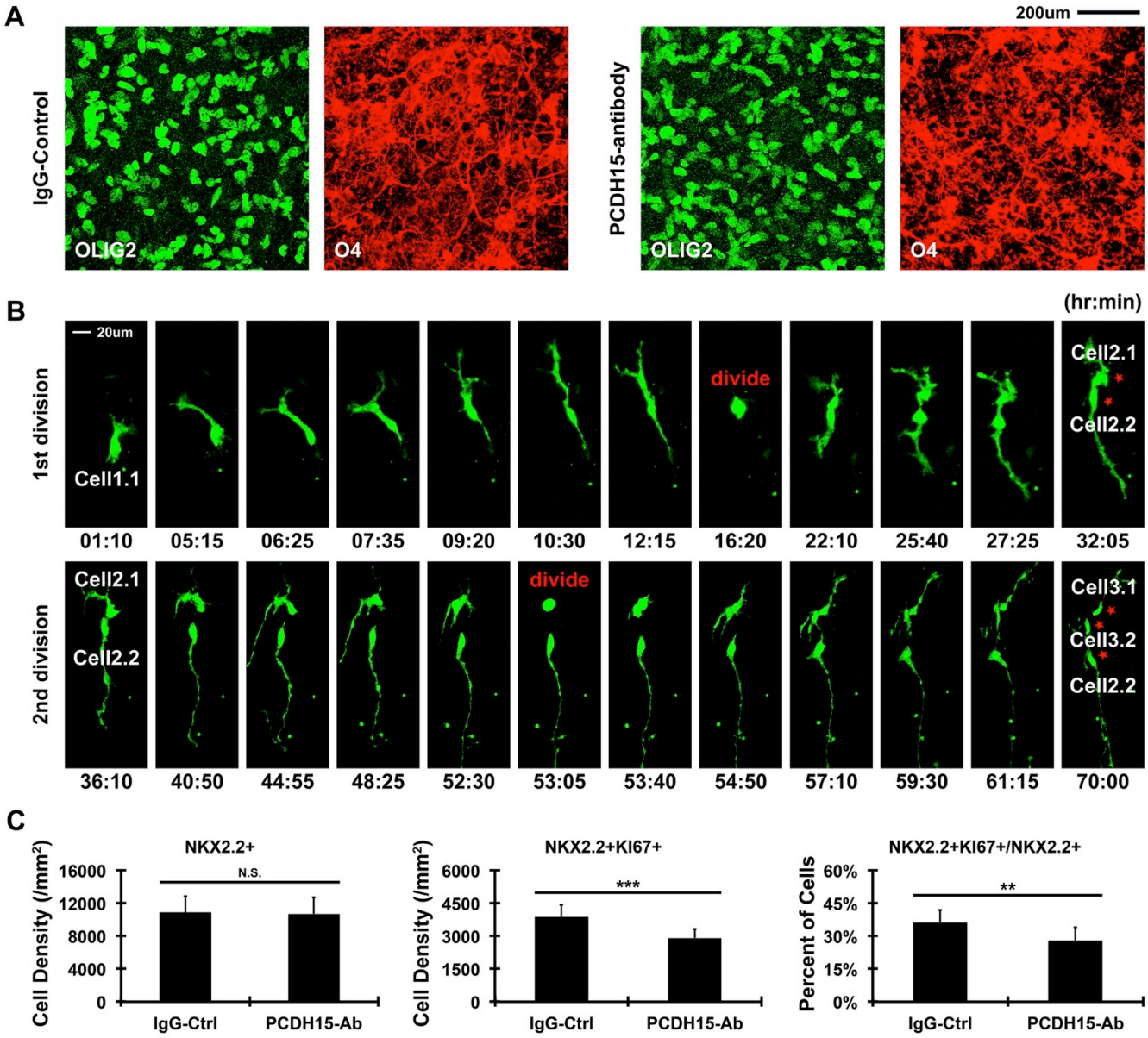
A
200um
IgG-Control
OLIG2
O4
PCDH15-antibody
OLIG2
O4
B
(hr:min)
20um
1st division
Cell1.1
divide
Cell2.1
Cell2.2
01:10
05:15
06:25
07:35
09:20
10:30
12:15
16:20
22:10
25:40
27:25
32:05
2nd division
Cell2.1
Cell2.2
divide
Cell3.1
Cell3.2
Cell2.2
36:10
40:50
44:55
48:25
52:30
53:05
53:40
54:50
57:10
59:30
61:15
70:00
C
NKX2.2+
Cell Density (/mm2)
16000
12000
8000
4000
0
N.S.
IgG-Ctrl
PCDH15-Ab
NKX2.2+KI67+
Cell Density (/mm2)
6000
4500
3000
1500
0
***
IgG-Ctrl
PCDH15-Ab
NKX2.2+KI67+/NKX2.2+
Percent of Cells
60%
45%
30%
15%
0%
**
IgG-Ctrl
PCDH15-Ab

Figure 7. Interfering with PCDH15 Function Affects OPC Proliferation.
(A) Sample images of OPCs in the OSVZ of cultured brain slices treated with either IgG as control, or PCDH15-antibody to interfere with PCDH15 function. Blocking to PCDH15 function did not cause obvious change in OPC morphology (indicated by O4-staining) and distribution (indicated by OLIG2-staining).
(B) Time stamped still images of dividing OPCs infected with *PCDH15*-shRNA lentiviruses. Two rounds of continuous division were observed, and only one of the daughter cells divided again. Representative cells are from cultured cortical slices at GW20-24 (n=6).
(C) Quantification of OPC division in the OSVZ of cultured brain slices treated with either IgG as control or PCDH15-antibody to interfere with PCDH15 function. Blocking to PCDH15 function inhibited OPC proliferation but did not change local OPC density. Mean±SD (n=6). (***, $p<0.001$; **, $p<0.01$; N.S., $p>0.05$.)
See also Movie S8-S9.

STAR*METHODS

Detailed methods are provided in the online version of this paper and include the following:

- KEY RESOURCES TABLE
- CONTACT FOR REAGENT AND RESOURCE SHARING
- EXPERIMENTAL MODEL AND SUBJECT DETAILS
  - Embryonic Human Brain Tissue Samples
- METHOD DETAILS
  - Immunohistochemistry
  - Primary Cell Dissociation and Immunopanning
  - Primary Cell Culture
  - Primary Organotypic Slice Cultures
  - Time Lapse Image
  - Sing-cell RNA-sequencing
  - Alignment
  - Sing-cell Clustering and Visualization
  - Monocle
  - shRNA Efficiency Test
  - Antibody Binding Test by FACS
- QUANTIFICATION AND STATISTICAL ANALYSIS
- DATA AND SOFTWARE AVAILABILITY

SUPPLEMENTAL INFORMATION

Supplemental Information includes five figures, and nine movies.

STAR*METHODS

KEY RESOURCES TABLE

REAGENT or RESOURCE	SOURCE	IDENTIFIER
Antibodies for Immunopanning		
Mouse monoclonal anti-PDGFRA	BD Biosciences	Cat.# 556001
Mouse monoclonal anti-O4	Millipore	Cat.# MAB345
Rat monoclonal anti-EGFR	Abcam	Cat.# ab231
Mouse monoclonal anti-LIFR	Abcam	Cat.# ab89792
Donkey anti-Mouse IgG	Jackson Immuno	Cat.# 715-005-151
Donkey anti-Mouse IgM	Jackson Immuno	Cat.# 715-005-020
Goat anti-Rat IgG	Jackson Immuno	Cat.# 112-005-003
Antibodies for Immunohistochemistry		
Rabbit anti-PDGFRA, 1:500	Cell Signaling	Cat.# 3174S
Mouse anti-PDGFRA, 1:200	BD Biosciences	Cat.# 556001
Goat anti-PDGFRA, 1:500	R&D Systems	Cat.# AF-307-NA
Rabbit anti-NG2, 1:100	Millipore	Cat.# AB5320
Rabbit anti-OLIG2, 1:500	Millipore	Cat.# AB9610
Mouse anti-OLIG2, 1:200	Millipore	Cat.# MABN50
Goat anti-OLIG2, 1:200	R&D Systems	Cat.# AF2418
Mouse anti-NKX2-2, 1:200	Abcam	Cat.# ab187375
Rabbit anti-EGFR, 1:500	Abcam	Cat.# ab32077
Sheep anti-EGFR, 1:500	Abcam	Cat.# ab98133
Mouse anti-SOX2, 1:300	BD Biosciences	Cat.# 561506
Goat anti-SOX2, 1:300	Santa Cruz	Cat.# sc-17320
Rabbit anti-PTPRZ1, 1:500	Atlas Antibodies	Cat.# HPA015103
Mouse anti-TNC, 1:100	Santa Cruz	Cat.# sc-25328
Rabbit anti-HOPX, 1:500	Proteintech	Cat.# 11419-1-AP
Rabbit anti-pS6, 1:300	Cell Signaling	Cat.# 2211S
Mouse anti-NES, 1:200	Millipore	Cat.# MAB5326

Rat anti-GFAP, 1:1000	Invitrogen	Cat.# 13-0300
Chicken anti-VIM, 1:1000	Millipore	Cat.# AB5733
Mouse anti-pVIM (Ser55), 1:500	MBL	Cat.# D076-3
Mouse anti-pVIM (Ser82), 1:500	MBL	Cat.# D095-3
Sheep anti-EOMES, 1:300	R&D Systems	Cat.# AF6166
Rabbit anti-PPP1R17, 1:300	Atlas Antibodies	Cat.# HPA047819
Mouse anti-KI67, 1:200	Dako	Cat.# M7240
Chicken anti-GFP, 1:1000	Abcam	Cat.# ab13970
Rat anti-BrdU (CldU), 1:500	BIO-RAD	Cat.# OBT0030G
Mouse anti-IdU, 1:200	Sigma-Aldrich	Cat.# SAB3701448
Antibody for Blocking		
Sheep anti-PCDH15	Invitrogen	Cat.# PA5-47865
Bacterial and Virus Strains		
CMV-GFP adenovirus	Vector Biolabs	Cat. # 1060
PCDH15-shRNA lenti-virus	Origene	Cat.# TL302649V
DSCAM-shRNA lenti-virus	Origene	Cat.# TL304905V
Chemicals, Peptides, and Recombinant Proteins		
Iressa	Tocris	Cat.# 3000
AG1478	Tocris	Cat.# 1276
PD153035	Tocris	Cat.# 1037
LIF	Peprotech	Cat.# 300-05
EGF	Peprotech	Cat.# 100-47
PDGF	Peprotech	Cat.# 100-13A
CNTF	Peprotech	Cat.# 450-13
NT-3	Peprotech	Cat.# 450-03
Kits for Single-cell RNA-sequencing		
C1 Single-Cell Auto Prep Integrated Fluidic Circuit (Fluidigm)		
SMARTer Ultra Low RNA Kit (Clontech)		
Nextera XT DNA Sample Preparation Kit (Illumina)		
Chromium Chip B Single Cell Kit (10X Genomics)		

CONTACT FOR REAGENT AND RESOURCE SHARING

Further information and requests for resources and reagents for resources and reagents should be directed to and will be fulfilled by the Lead Contact, Arnold R Kriegstein (Arnold.Kriegstein@ucsf.edu).

EXPERIMENTAL MODEL AND SUBJECT DETAILS

Embryonic Human Brain Tissue Samples

De-identified tissue samples were collected with previous patient consent in strict observance of the legal and institutional ethical regulations from elective pregnancy termination specimens at San Francisco General Hospital. Protocols were approved by the Human Gamete, Embryo and Stem Cell Research Committee (institutional review board) at the University of California, San Francisco. Human brain tissue was transported to the laboratory within 2h of collection in artificial cerebrospinal fluid containing 125mM NaCl, 2.5mM KCl, 1mM $MgCl_2$, 1mM $CaCl_2$, 1.25mM NaH_2PO_4, 25mm $NaHCO_3$, 25mm D-glucose, bubbled with 95% O_2 and 5% CO_2.

METHOD DETAILS

Immunohistochemistry

Primary tissue samples were cut into 1cm3 pieces and fixed in 4% PFA in Ca2+/Mg2+ free PBS (pH=7.4) for 1h at room temperature or overnight at 4°C with constant agitation. After fixation, they were washed in PBS, equilibrated in 30% sucrose in PBS overnight at 4°C, embedded in blocks with a 1:1 mixture of 30% sucrose / OCT compound (Tissue-Tek, VWR) and frozen at -80°C. Blocks were frozen sectioned to a thickness of 16-20um cyosections. Antigen retrieval was performed if necessary, by heating section to 95°C in 10mM sodium citrate (pH=6) for 20min. Sections were then permeablized and blocked with 10% donkey serum in PBS with 0.1% Triton X-100 and 0.2% gelatin. Primary antibody incubations were performed at 4°C overnight, followed by three times of 10min PBS wash, and AlexaFluor secondary antibody (Thermo Fisher, 1:500 dilution) with DAPI incubations were performed at room temperature for 3hr. To detect thymidine analogs (BrdU, CldU or IdU), sections were denatured with 2N HCl for 1hr at room temperature followed by neutralization with 0.1M boric acid, and incubated with primary and secondary antibodies as described above. Slides were mounted with Aqua-mount (Lerner Laboratories). For quantitative analysis of cell numbers in

Figure S1-S4, samples were from 2 to 3 independent biological individuals, and 6 fields of microscrope images from each individual at each position (VZ/ISVZ/OSVZ/IZ/SP/CP) were included. For quantitative analysis of cell numbers in Figure 5B, 10 fields of microscrope images from each individual were included and the experiment was repeated in 3 independent biological individuals.

Primary Cell Dissociation and Immunopanning

Tissue samples were dissected in artificial cerebrospinal fluid using a microsurgical blade under a stereotaxic dissection microscope (Leica). To obtain single cell suspension, tissue samples were further cut into small pieces (<1mm^3) and placed in a 6cm dish containing a pre-warmed solution of Papain and DNase freshly diluted in Earl's Balanced Salt Solution that was prepared according to the manufacturer protocol (Worthington Biochemical Corporation). After incubation at 37°C for 1h, tissue was centrifuged at 220g for 1 min to remove the Papain/DNase supernatant, washed with a OVO protease inhibitor stock solution. After centrifugation at 220g for 10min, and resuspension in Dulbecco's Modified Eagle Medium / Nutrient Mixture F-12, tissue was further gently triturated by pipetting up and down approximately 10 times into a single cells suspension. The cell suspension was then added to a series of plastic Petri dishes pre-coated with cell-type-specific antibodies and incubated at 37°C for 30min to 1h each. Unbound cells were transferred to the subsequent Petri dish; while the dish with bound cells was rinsed 10 times with DPBS to wash away loosely bound contaminating cell types. Bound cells were digested with 0.05% trypsin/EDTA, centrifuge at 220g for 15min, and resuspended in corresponding medium.

Primary Cell Culture

Culture chamber slides were prepared by overnight coating with 0.01% poly-L-ornithine (Millipore Sigma) at 37°C. After three water washes, plates were coated with 5ug/ml laminin (Thermo Fisher) and 1ug/ml fibronectin (Corning) for 2hr. Single cell suspension was plated in the culture chamber slides at the concentration of 10^5/well for 8 well chambers or $2X10^5$/well for 4 well chambers. Cells were cultured in the medium containing N2 supplement (1:100, Thermo FIsher), B27 supplement (1:50, Thermo Fisher), LIF (20ng/ml, Peprotech), EGF (20ng/ml, Peprotech), Insulin (5ug/ml, Sigma), Penicillin/Streptomycin (100U/ml) in

DMEM/F12+GlutamaxTM-I (Thermo Fisher) for the first 2 days, and then in the medium containing N2 supplement, B27 supplement, Insulin, NAC (5ug/ml, Sigma), Biotin (10ng/ml, Sigma), Trace Elements B (1000X, Thermo Fisher), CNTF (10ng/ml, Pepotech), PDGF (20ng/ml, Peprotech), NT-3 (1ng/ml, Peprotech), Penicillin/Streptomycin (100U/ml) in DMEM/F12+GlutamaxTM-I (Thermo Fisher) for the subsequent 5 or 8 days. Cells were incubated at 37°C, 5% CO_2. For quantitative analysis of cell numbers in Figure 3C and S5C, 5 fields of microscrope images from each individual were included and the experiment was repeated in 3 independent biological individuals.

Primary Organotypic Slice Cultures

Primary tissue samples were cut into 5mm thick pieces, and embedded in 3% low melting point agarose (Thermo Fisher) in artificial cerebrospinal fluid and sectioned into 250um using a Leica VT1200S vibrating blade microtome in artificial cerebrospinal fluid. Slices were then plated on Millicell inserts (Millipore) in the 6-well plate in the medium containing 60% Basal Medium Eagle (Thermo Fisher), 25% Hank's BSS (Thermo Fisher), 10% FBS (Thermo Fisher), 1% Penicillin/Streptomycin/Glutamine (Thermo Fisher), 1% N2 (Thermo Fisher), and 0.66% glucose. Slices were then cultured at 37°C, 5%CO2 and 8% O2 for up to 1 week. For pharmacological treatment assays, EGFR activator EGF was added into the slice culture medium at the final concentration of 50ng/ml [EGF(L)] or 200ng/ml [EGF(H)], while EGFR inhibitors Iressa, AG1478, and PD153035 were added into the slice culture medium at the final concentration of 50nM. For transplantation assays, primary cells were enriched by immunopanning, incubated with CMV-GFP adeno-virus for 1hr or shRNA lenti-virus for 3hr, washed in DPBS for twice, and injected into the cultured slices using a glass needle pipette. A total of 10^5 cells were evenly injected into 3 pieces of $1cm^2$ brain slices. For thymidine incubation assay, either CldU, IdU, or BrdU was added into the slice culture medium at the final concentration of 10nM for 12hr, and three iterations of PBS washing were performed after each thymidine treatment. For quantitative analysis of cell numbers in Figure 3D, 4E, and 7C, 6 fields of microscrope images under each treatment from each individual were included and the experiment was repeated in 3 independent biological individuals.

Time Lapse Image

After 2-3 days culture, GFP-expressing brain slices were transferred into glass-bottom plate with fresh medium, placed to an inverted Leica TCS SP5 with an on-stage incubator streaming 5% CO_2, 8% O_2, balance N_2 into the chamber. Slices were imaged for GFP using a 10X air objective (Zoom 2X) at 35 min intervals for up to 3 or 5 days with repositioning of the z-stacks every 24hr. For quantitative analysis in Figure 4D and 6DE, 30 cells from 2-3 independent biological individuals were pooled together.

Single-cell RNA-sequencing

For Fluidigm C1 scRNA-seq, cDNA synthesis and pre-amplification were performed as described before (Nowakowski et al., Science, 2017) using Fluidigm C1 auto-prep system following manufacturer's protocol. After capture, microscope imaging was performed to identify wells with either debris or doublets and retain single-cell wells; these identifications were used in downstream analysis. Library preparation was performed using the Illumina Nextera XT library preparation kit. Library concentration quantification was performed using Bioanalyzer (Agilent). Paired-end 100bp sequencing was performed on the Illumina HiSeq2500.

For 10X Genomics scRNA-seq, target capture of 10,000 cells per sample was used; cDNA synthesis, pre-amplification and library preparation were performed as described before (Bhaduri et al., Nature, 2020) following manufacturer's protocol "User Guide: Chromium Single Cell 3' Reagent Kits (V3 Chemistry)". Libraries from individual samples were pooled and sequenced on the NovaSeq 6000 machine.

Alignment

Trim Galore 3.7 was used to trim 20 bp of adaptor sequencing, and paired-end alignments were performed using HISAT2 to the human reference genome GRCh38. Counts for each cell were performed using subread-1.5.0 function featureCounts. After counts were obtained, normalization to counts per million was performed. Quality control was performed to further ensure that only high quality single cell data was processed further, and cells with fewer than 1000 genes/cell were removed, as were cells with greater than 10% of their individual transcriptome represented in either mitochondrial or ribosomal transcripts. Only genes expressed in at least 30 cells were carried forward in the analysis.

Single-cell Clustering and Visualization

Principal component analysis (PCA) was used to reduce the dimensionality of the dataset, and clustering was performed as previously described (Shekhar et al, 2016). In PC space, for each cell, the top 30 nearest neighbors were calculated for each cell using the 'RANN' R package nn2 function. The Jaccard distance, a weighted distance metric based upon the mutually shared neighbor sets for each pair of neighboring cells was calculated prior to clustering. With the Jaccard weighted distances, louvain clustering was performed using the 'igraph' R package. TSNE coordinates were calculated in PCA space (independent of the clusters). Differential expression to identify cluster markers was performed using the FindAllMarkers function in Seurat. The heatmap was generated using key marker genes in the space of a subset of clusters relevant to the analysis. The similarity matrix was calculated by correlating clusters to one another in principal component space.

Monocle

Monocle version 2 was used to generate the trajectory analysis. Excitatory neurons, IPCs, RGCs, and OPCs were extracted based upon the above clustering. These cells were re-clustered as above and used as the input to Monocle. Differential gene expression for trajectory construction was performed using these cluster annotations, and metadata of broad cell type was used to color the plot.

shRNA Efficiency Test

HEK293T cells were plated in 12-well plates, and 200ng of cDNA vectors of PCDH15 (NM_001142763.1, Sino Biological HG18931-UT) or DSCAM (NM_001271534.1, Sino Biological HG19944-UT) with 600ng of corresponding shRNA vectors were transfected into the cells using Lipofectamine 3000. Cells were harvested 48 hours after transfection for mRNA extraction using the RNAeasy micro plus kit. RNA quantity and quality were checked using NanoDrop 1000 (Thermo Scientific). qRT-PCR was performed using the ViiA 7 Real-time PCR System with PowerUp SYBR Green Master Mix, and analyzed with comparative Ct method normalized against the housekeeping gene GAPDH. Cells were harvested 72 hours after transfection for protein extraction. Cells were lysed with RIPA buffer (50 mM Tris-HCl pH 8.0, 150 mM NaCl, 1 mM EDTA, 1 % NP-40, 0.5% sodium deoxycholate, 0.1% SDS)

supplemented with phosphatase and protease inhibitors (Roche). Lysates were homogenized by sonication followed by protein quantification via BCA assay (Pierce). LDS Sample buffer (Invitrogen) with a reducing agent was added to each lysate followed by a 10 min incubation at 95°C. Samples were spun down and electrophoresed on a 4–12% Bis-Tris gel, transferred to a nitrocellulose membrane and blocked for one hour with Intercept (TBS) Protein-Free Blocking Buffer (LI-COR) prior to primary antibody incubation o/n. After 1-hour secondary antibody incubation the next day, membranes were imaged using an Odyssey Infrared Imager (LI-COR).

Additionally, OPCs were enriched by PDGFRA-immunopanning and cultured in 12-well plates (for qRT-PCR) or 6-well plate (for western blotting). When the cell density reached 80% of coverage, cells were infected with PCDH15-shRNA or DSCAM-shRNA lenti-viruses. OPCs were harvest three days after infection for qRT-PCR, or five days after infection for western blotting.

Antibody Binding Test by FACS

HEK293T cells were seeded into 6-well plates, and 1ug PCDH15 (NM_001142763.1, Sino Biological HG18931-UT), PCDH9 (Dharmacon OHS6085-213579205), or PCHD17 (Dharmacon MHS6278-202801988) cDNA vectors were transfected into the cells using Lipofectamine 3000. For flow cytometry analysis to assay antibody specificity, cells were released 72 hours after cDNA transfection using PBS-EDTA (Lonza). 2 x 10^6 cells per condition were used for PCDH15 primary antibody (R&D systems AF6729, 1:40) staining in FACS staining buffer (D-PBS, 1% BSA, 2mM EDTA, 0.1% sodium azide) for 30 minutes on ice. Next, cells were washed in FACS staining buffer and incubated with Alexa Fluor 488 conjugated secondary antibodies (Invitrogen, 1:400) for 30 minutes on ice. After final washes, Sytox Red (Invitrogen, 1:1000) was added to stain dead cells. Flow cytometry was carried out on an BD LSRFortessa X-20.

QUANTIFICATION AND STATISTICAL ANALYSIS

Quantification of images was performed using the Imaris Image Analysis software (Bitplane). Statistical analysis was performed using Microsoft Excel. Statistical tests, significance values, and experimental n are included in figure legends. All data are shown as mean ± SEM. In all

cases, p values are represented as follows: ***p<0.001, **p<0.01, *p<0.5, and N.S. when p>0.5.

For quantitative analysis of cell numbers in Figure S1-S4, samples were from 2 to 3 independent biological individuals, and 6 fields of microscrope images from each individual at each position (VZ/ISVZ/OSVZ/IZ/SP/CP) were included. For quantitative analysis of cell numbers in Figure 3C and S5C, 5 fields of microscrope images from each individual were included and the experiment was repeated in 3 independent biological individuals. For quantitative analysis of cell numbers in Figure 3D, 4E, and 7C, 6 fields of microscrope images under each treatment from each individual were included and the experiment was repeated in 3 independent biological individuals. For quantitative analysis of cell numbers in Figure 5B, 10 fields of microscrope images from each individual were included and the experiment was repeated in 3 independent biological individuals. For quantitative analysis in Figure 4D and 6DE, 30 cells from 2-3 independent biological individuals were pooled together.

DATA AND SOFTWARE AVAILABILITY

The sequencing data have been deposited in GEO under ID code GEO:

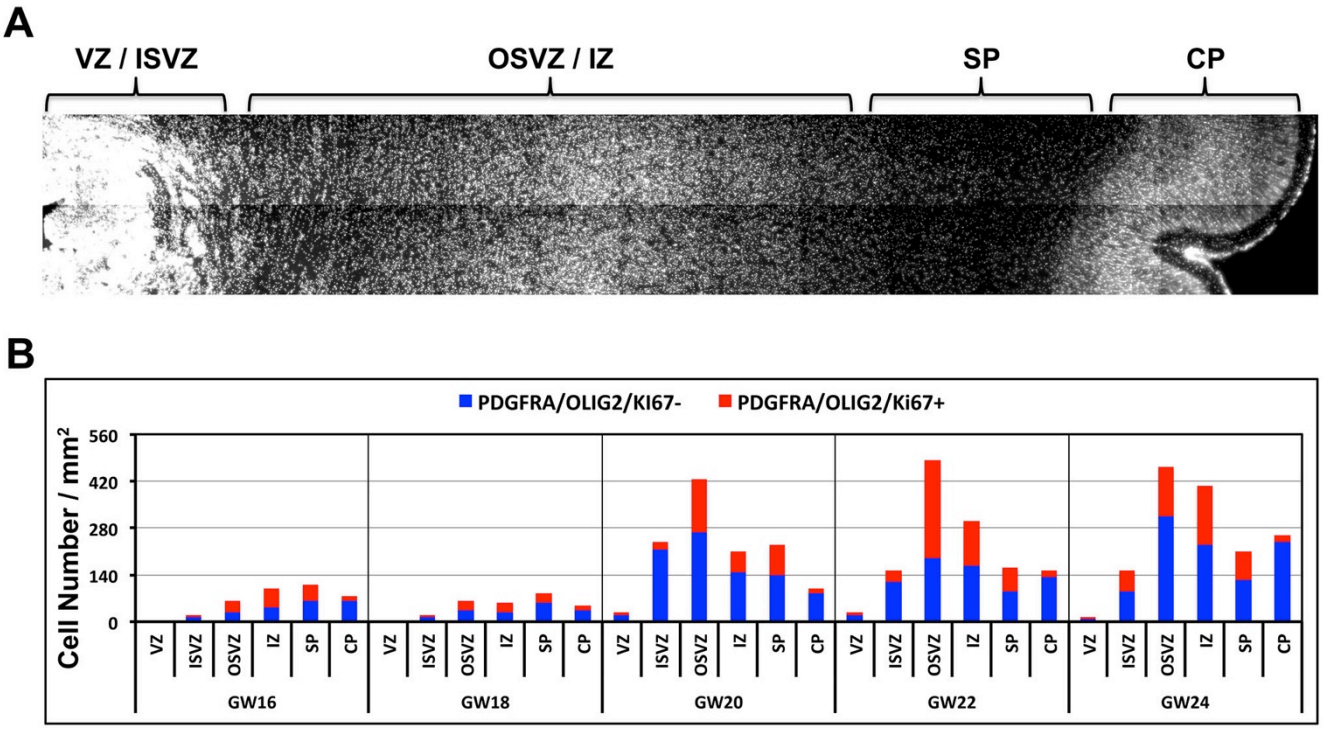
A
VZ / ISVZ
OSVZ / IZ
SP
CP
B
PDGFRA/OLIG2/KI67-
PDGFRA/OLIG2/Ki67+
Cell Number / mm2
560
420
280
140
0
VZ
ISVZ
OSVZ
IZ
SP
CP
GW16
GW18
GW20
GW22
GW24
C
DAPI
PDGFRA - OLIG2 - KI67
OSVZ
VZ
100um

Figure S1. Co-staining of PDGFRA, OLIG2, and KI67, Related to Figure 3 and 5.
(A) DAPI stained cortical slice with signposts showing how laminar regions were designated. (VZ: ventricular zone; ISVZ: inner subventricular zone; OSVZ: outer subventricular zone; IZ: intermediate zone; SP: subplate; CP: cortical plate.)
(B) Quantification of $PDGFRA^{+}OLIG2^{+}$ OPC number in different cortical laminae at different time points in late second trimester, with $KI67^{-}$ cells in blue and $KI67^{+}$ cells in red. At each stage (GW16/18/20/22/24), samples were from 2 to 3 individuals and 6 fields of microscropic images from each individual at each position (VZ/ISVZ/OSVZ/IZ/SP/CP) were included.
(C) Representative images of PDGFRA, OLIG2, and KI67 co-staining at GW22.

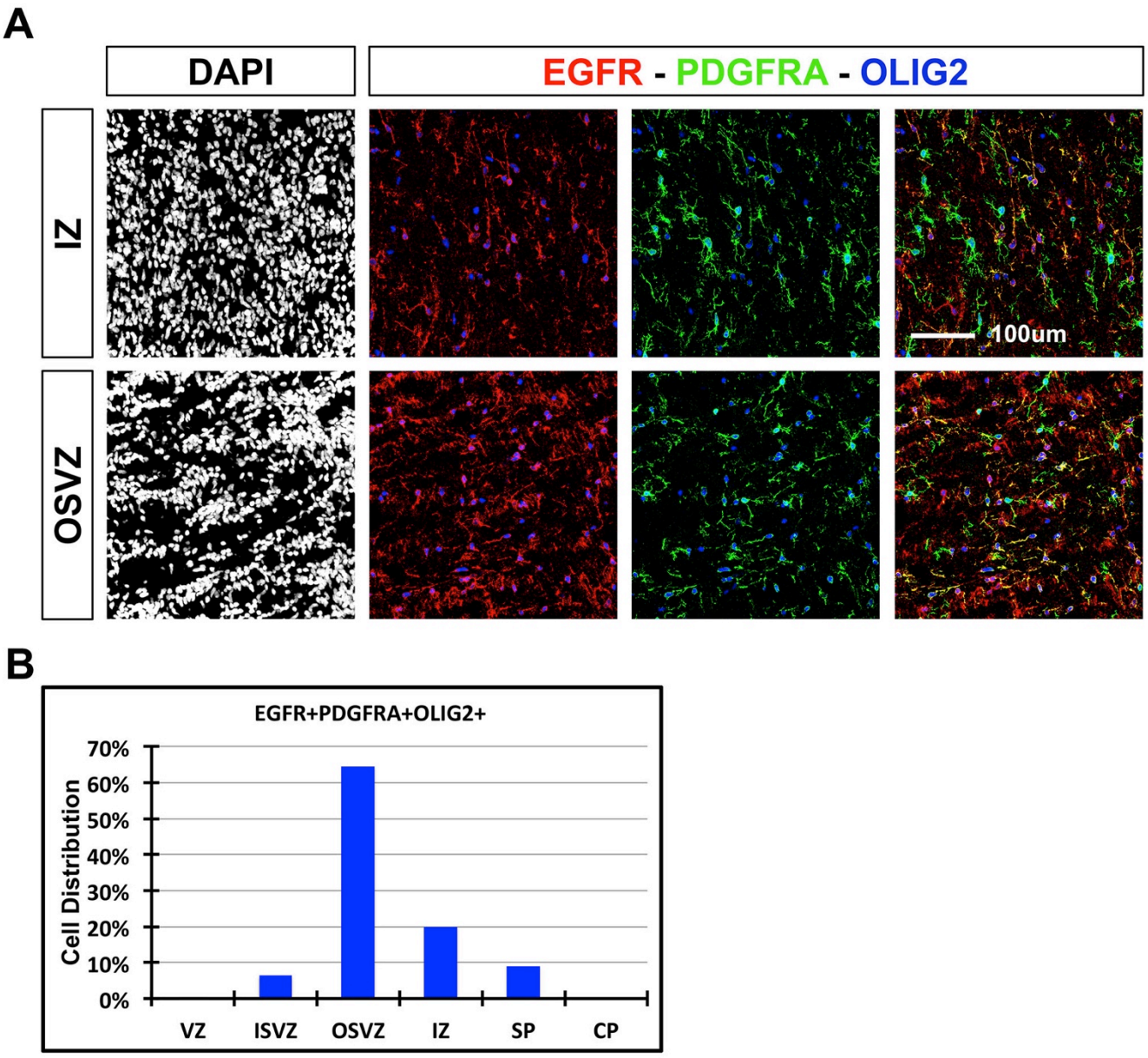

Figure S2. Co-staining of EGFR, PDGFRA, and OLIG2, Related to Figure 3.
(A) Representative images of EGFR, PDGFRA, and OLIG2 co-staining at GW22.
(B) Distribution analysis of $EGFR^{+}PDGFRA^{+}OLIG2^{+}$ cells across different cortical laminae at GW22. These triple labeled cells represent a transition stage from NPC to OPCs. Samples from 3 individuals and 6 fields of microscopic images from each individual at each position (VZ/ISVZ/OSVZ/IZ/SP/CP) were included.

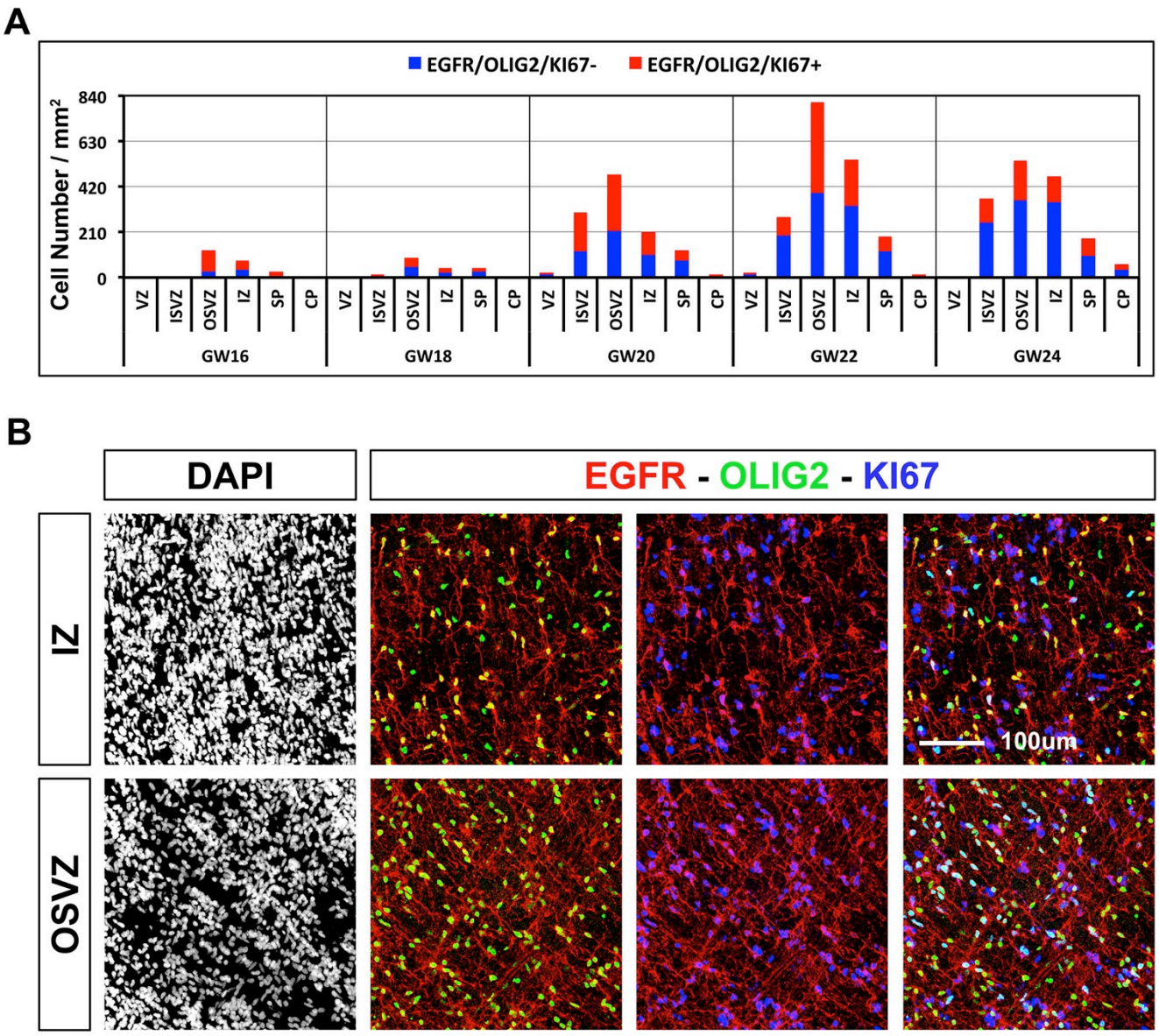

Figure S3. Co-staining of EGFR, OLIG2, and KI67, Related to Figure 3.
(A) Quantification of $EGFR^{+}OLIG2^{+}$ Pre-OPC number in different cortical laminae at different time points in late second trimester, with $KI67^{-}$ cells in blue and $KI67^{+}$ cells in red. At each stage (GW16/18/20/22/24), samples were from 2 to 3 individuals and 6 fields of microscopic images from each individual at each position (VZ/ISVZ/OSVZ/IZ/SP/CP) were included.
(B) Representative images of EGFR, OLIG2, and KI67 co-staining at GW22.

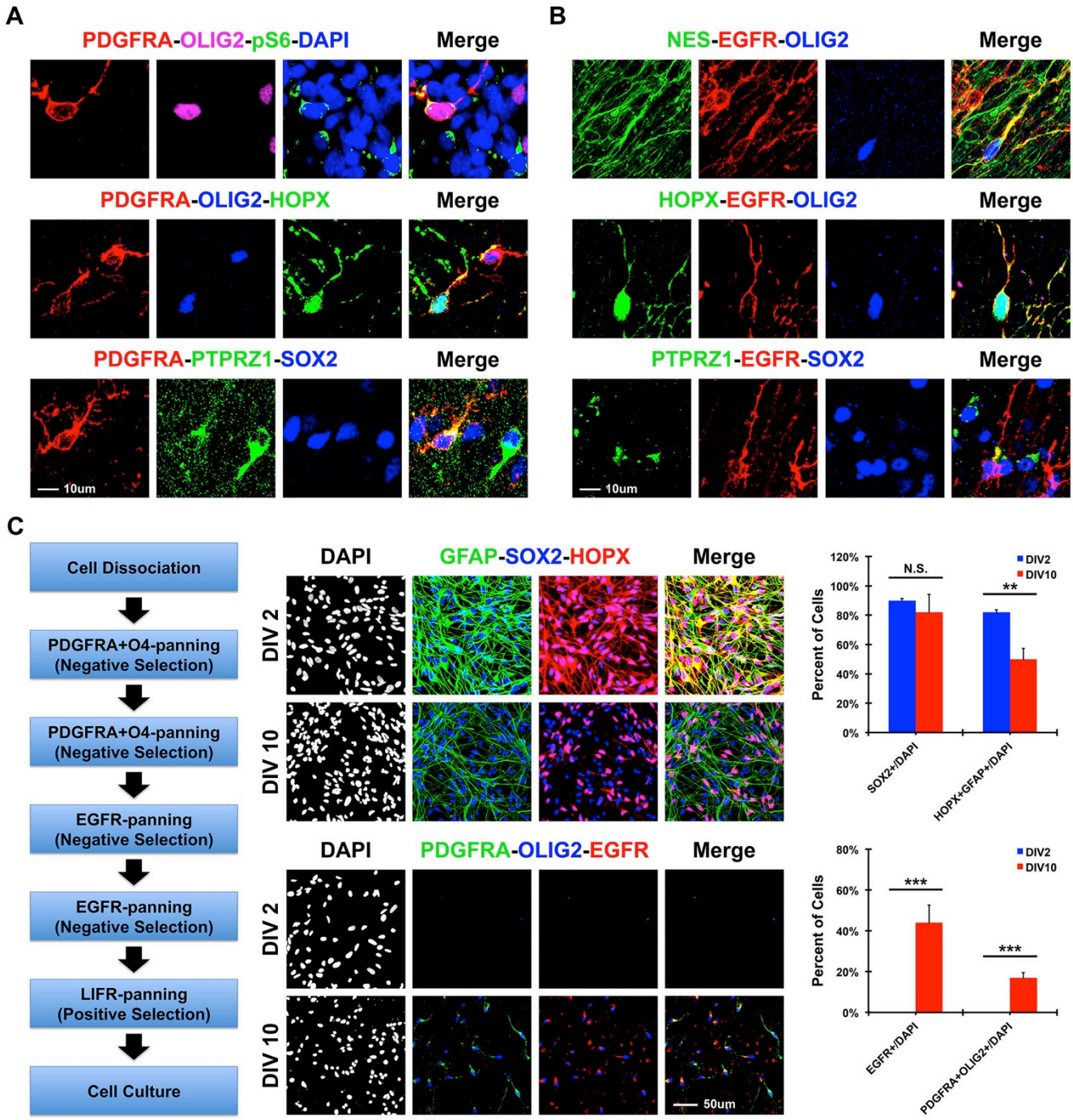
A
PDGFRA-OLIG2-pS6-DAPI
Merge
PDGFRA-OLIG2-HOPX
Merge
PDGFRA-PTPRZ1-SOX2
Merge
10um
B
NES-EGFR-OLIG2
Merge
HOPX-EGFR-OLIG2
Merge
PTPRZ1-EGFR-SOX2
Merge
10um
C
Cell Dissociation
PDGFRA+O4-panning (Negative Selection)
PDGFRA+O4-panning (Negative Selection)
EGFR-panning (Negative Selection)
EGFR-panning (Negative Selection)
LIFR-panning (Positive Selection)
Cell Culture
DAPI
GFAP-SOX2-HOPX
Merge
DIV 2
DIV 10
DAPI
PDGFRA-OLIG2-EGFR
Merge
DIV 2
DIV 10
50um
Percent of Cells
120%
100%
80%
60%
40%
20%
0%
N.S.
**
DIV2
DIV10
SOX2+/DAPI
HOPX+GFAP+/DAPI
Percent of Cells
80%
60%
40%
20%
0%
***
***
DIV2
DIV10
EGFR+/DAPI
PDGFRA+OLIG2+/DAPI

Figure S4. Outer Radial Glia Cells Generate OPCs through EGFR-expressing Pre-OPCs. Related to Figure 3 and 4.

(A) Characterization of cells co-expressing oRG and OPC markers. Images from human OSVZ at GW20-24 (n=3).

(B) Characterization of cells co-expressing oRG markers and EGFR. Images from human OSVZ at GW20-24 (n=5).

(C) Outline of immunopanning workflow (left). Cells were micro-dissected from human OSVZ. PDGFRA and O4 were used to deplete OPCs, and EGFR was used to deplete Pre-OPCs. LIFR positive selection enriched for oRGs. Images of marker staining at DIV2 and DIV10 showing lineage progression (middle). Quantification of cell proportions (right). Mean±SD (n=5). (***, $p<0.001$; **, $p<0.01$; *, $p<0.05$; N.S., $p>0.05$.)

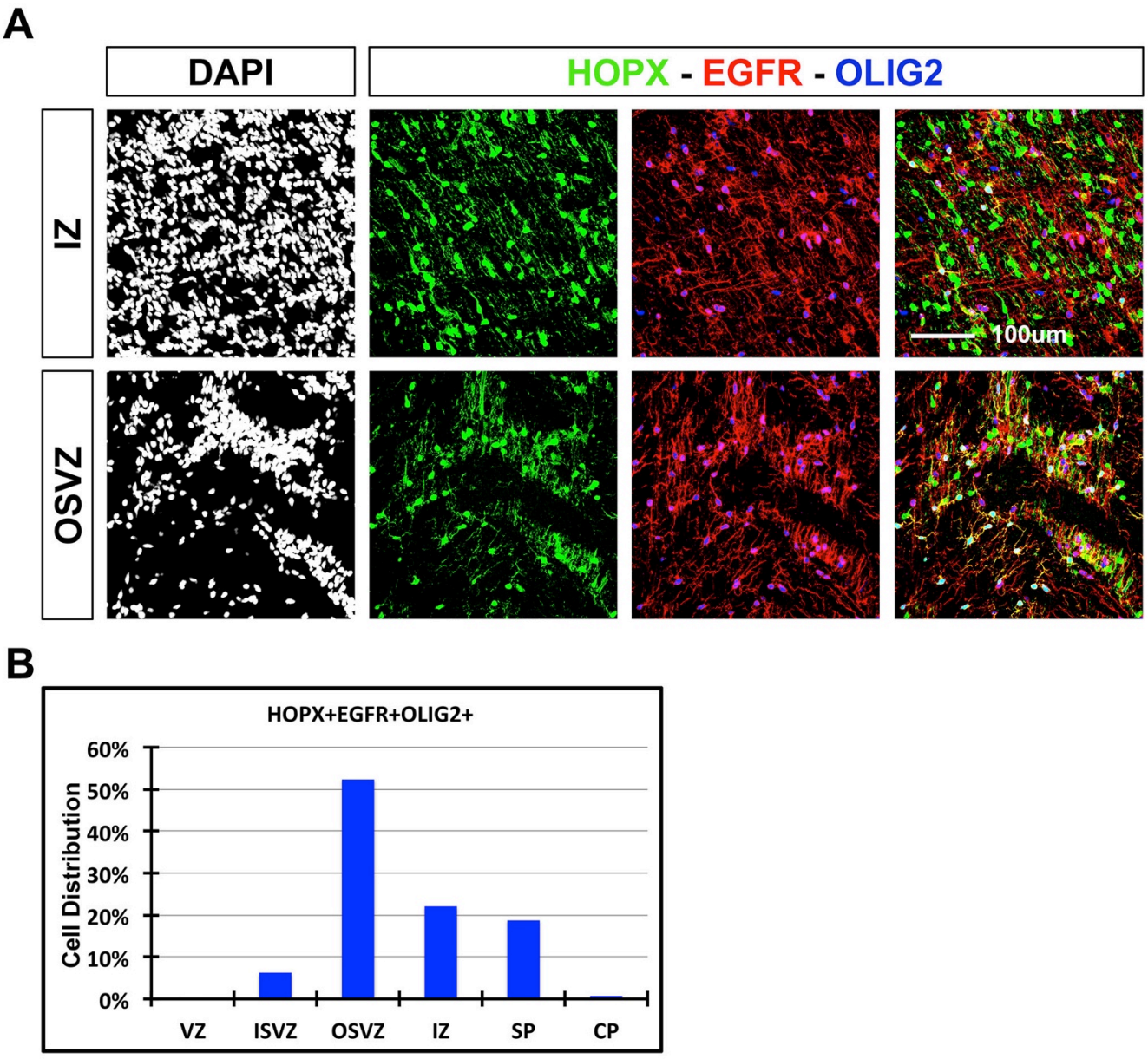

Figure S5. Co-staining of HOPX, EGFR, and OLIG2, Related to Figure 3.
(A) Representative images of HOPX, EGFR, and OLIG2 co-staining at GW22.
(B) Distribution analysis of $HOPX^{+}EGFR^{+}OLIG2^{+}$ cells across different cortical laminae at GW22. These triple labeled cells represent a transition stage from oRGs to Pre-OPCs. Samples from 3 individuals and 6 fields of microscopic images from each individual at each position (VZ/ISVZ/OSVZ/IZ/SP/CP) were included.

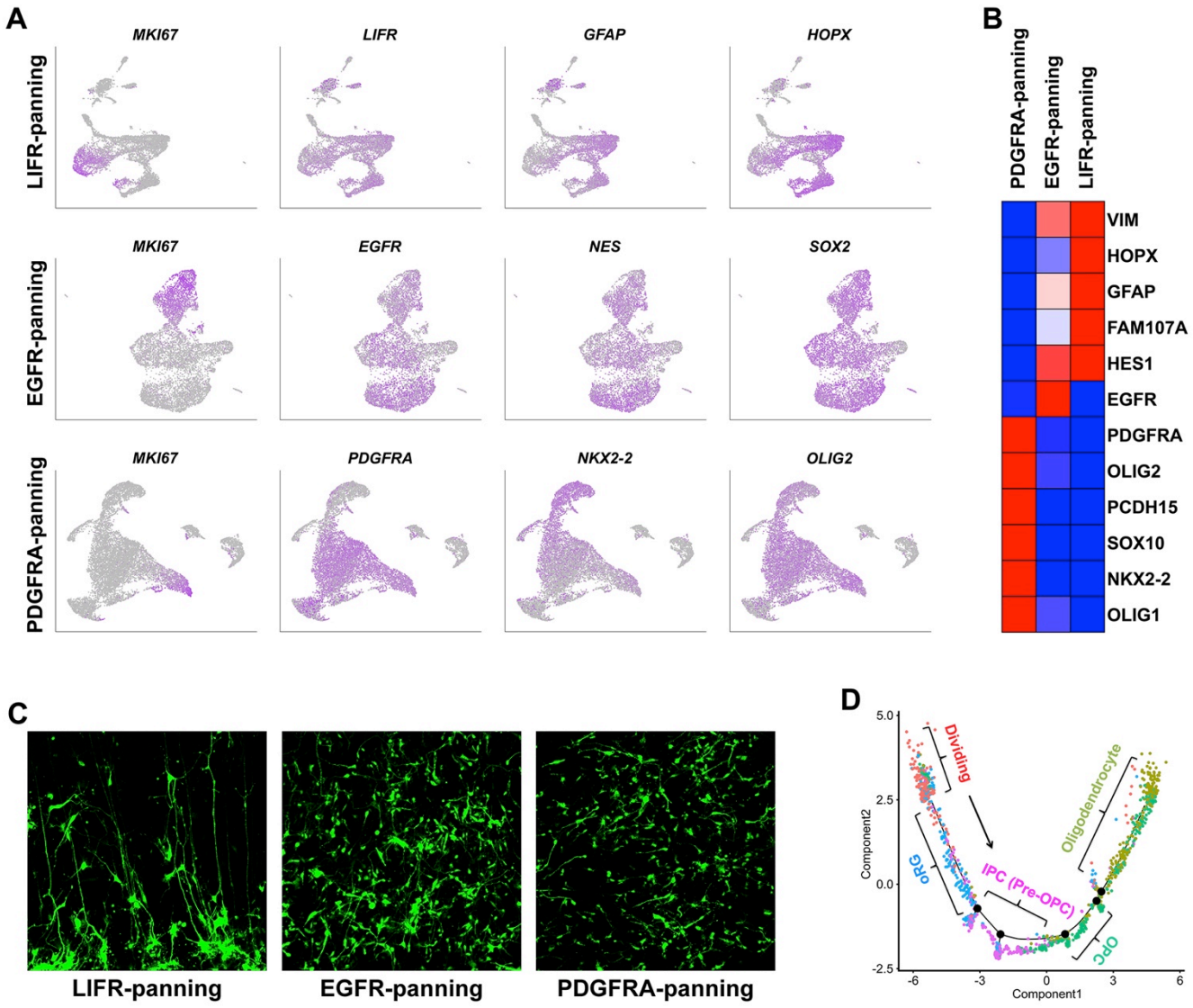

Figure S6. Validation of Immunopanning Strategy. Related to Figure 4.
(A) Feature plots of marker genes after 10X scRNA-seq. Cells were enriched by immunopanning and proliferative cells are indicated by MKI67 plots.
(B) Heatmap showing differential gene expression between cells immunopanned by different antibodies.
(C) Sample images of GFP virus infected cells enriched by immunopanning and transplanted to cultured cortical slices.
(D) Trajectory analysis of different progenitors from 10X scRNA-seq using Monocle. Broad cell types are shown rather than individual clusters.

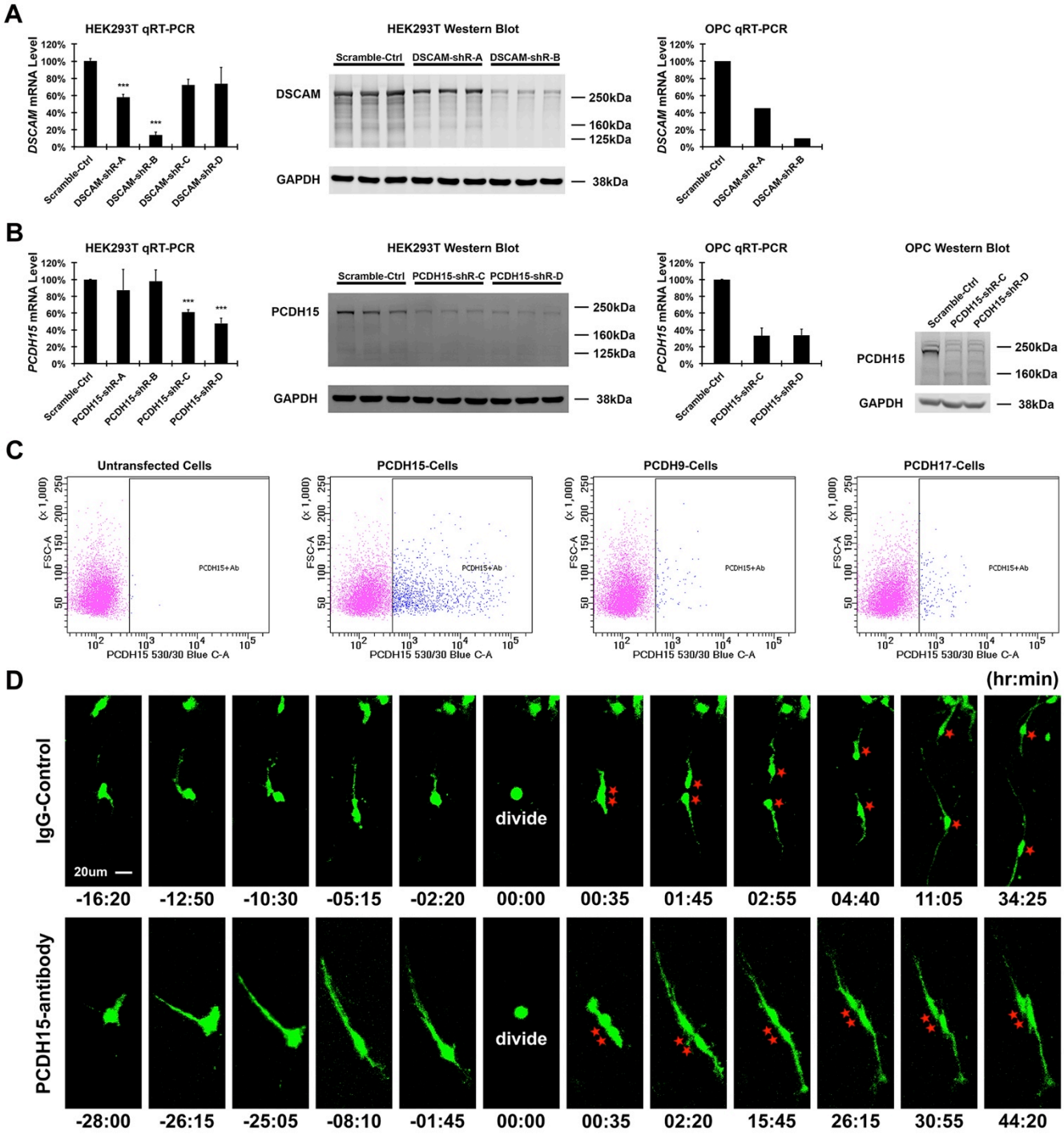
A
HEK293T qRT-PCR
DSCAM mRNA Level
120%
100%
80%
60%
40%
20%
0%
***
***
Scramble-Ctrl
DSCAM-shR-A
DSCAM-shR-B
DSCAM-shR-C
DSCAM-shR-D
HEK293T Western Blot
Scramble-Ctrl
DSCAM-shR-A
DSCAM-shR-B
DSCAM
250kDa
160kDa
125kDa
GAPDH
38kDa
OPC qRT-PCR
DSCAM mRNA Level
Scramble-Ctrl
DSCAM-shR-A
DSCAM-shR-B
B
HEK293T qRT-PCR
PCDH15 mRNA Level
Scramble-Ctrl
PCDH15-shR-A
PCDH15-shR-B
PCDH15-shR-C
PCDH15-shR-D
HEK293T Western Blot
Scramble-Ctrl
PCDH15-shR-C
PCDH15-shR-D
PCDH15
250kDa
160kDa
125kDa
GAPDH
38kDa
OPC qRT-PCR
PCDH15 mRNA Level
Scramble-Ctrl
PCDH15-shR-C
PCDH15-shR-D
OPC Western Blot
Scramble-Ctrl
PCDH15-shR-C
PCDH15-shR-D
PCDH15
250kDa
160kDa
GAPDH
38kDa
C
Untransfected Cells
PCDH15-Cells
PCDH9-Cells
PCDH17-Cells
FSC-A
(x 1,000)
PCDH15+Ab
PCDH15 530/30 Blue C-A
D
(hr:min)
IgG-Control
20um
divide
-16:20
-12:50
-10:30
-05:15
-02:20
00:00
00:35
01:45
02:55
04:40
11:05
34:25
PCDH15-antibody
divide
-28:00
-26:15
-25:05
-08:10
-01:45
00:00
00:35
02:20
15:45
26:15
30:55
44:20

Figure S7. Validation of RNA Interference and Antibody Treatment. Related to Figure 6.
(A) Validation of *DSCAM*-shRNA by RT-PCR and Western Blot.
(B) Validation of *PCDH15*-shRNA by RT-PCR and Western Blot.
(C) Validation of PCDH15-antibody extracellular-binding by FACS.
(D) Time stamped still images of dividing OPCs treated with either IgG as control or PCDH15-antibody to interfere with PCDH15 function. In each case, the control divisions resulted in repulsion between daughter cells. With PCDH15 interference, the daughter cells remained close to each other. Representative cells are from cultured cortical slices at GW20-24 (n=30).

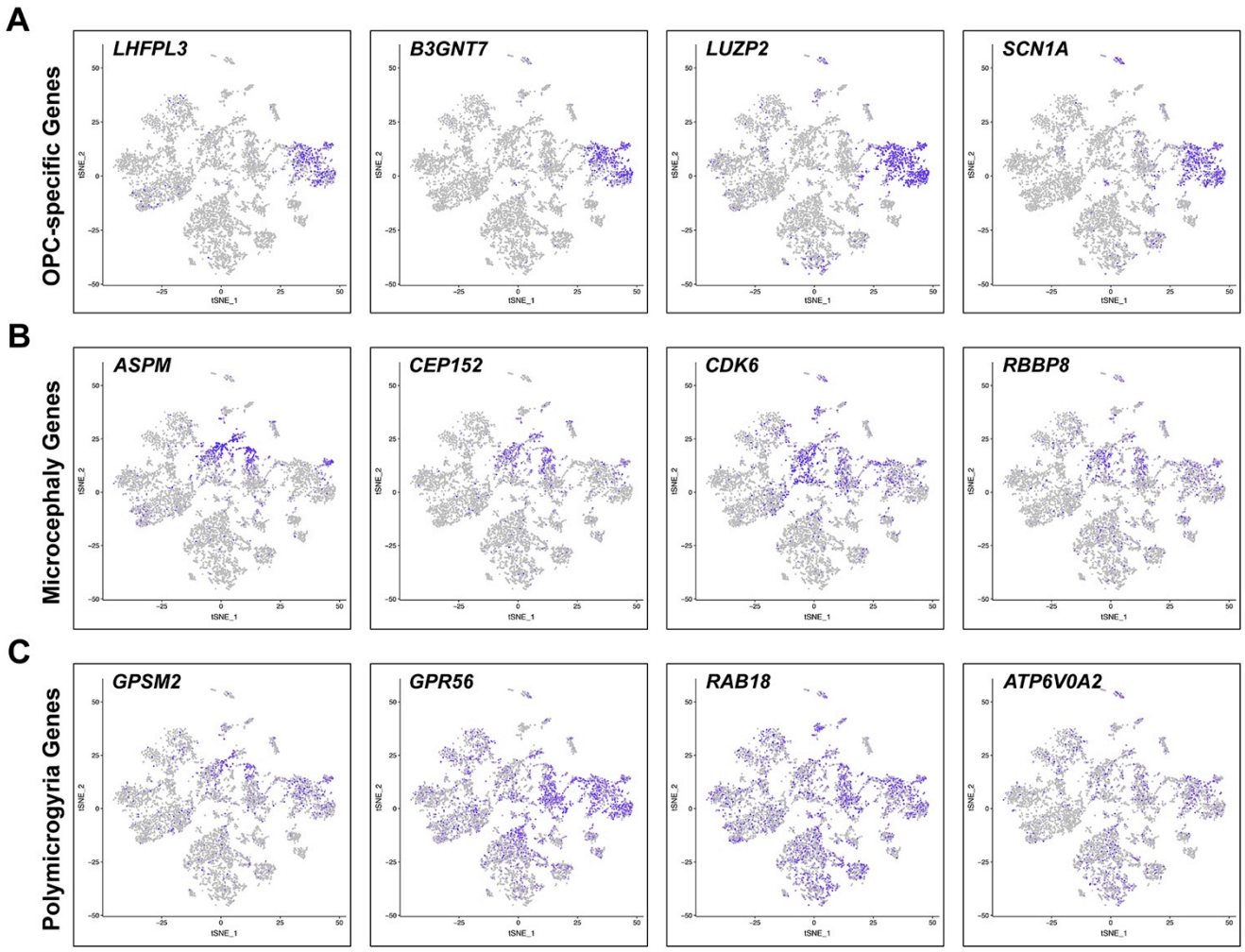

Figure S8. Representative Feature Plots of OPC-specific Genes and Cortical Malformation Related Genes.

Movie S1. Representative Video of an oRG Enriched by LIFR-panning. Related to Figure 4.

Movie S2. Representative Video of a Pre-OPC Enriched by EGFR-panning. Related to Figure 4.

Movie S3. Representative Video of an OPC Undergoing Two Rounds of Continuous Division. Related to Figure 5.

Movie S4. Representative Video of an OPC Infected with Scramble-shRNA Lentivirus, Related to Figure 6.

Movie S5. Representative Video of an OPC Infected with *PCDH15*-shRNA Lentivirus. Related to Figure 6.

Movie S6. Representative Video of an OPC Treated with IgG. Related to Figure S7.

Movie S7. Representative Video of an OPC Treated with PCDH15-antibody. Related to Figure S7.

Movie S8. Representative Video of Two OPCs Encountering Each Other. Related to Figure 7.

Movie S9. Representative Video of an OPC Infected with *PCDH15*-shRNA Lentivirus Undergoing Two Rounds of Continuous Division. Related to Figure 7.

REFERENCES

Aguirre, A., Dupreee, J.L., Mangin, J.M., and Gallo, V. (2007). A functional role for EGFR signaling in myelination and remyelination. Nat Neurosci. 10, 990-1002.

Barres, B.A. (2014). Designing and troubleshooting immunopanning protocols for purifying neural cells. Cold Spring Harb Protoc. 12, 1342-1347.

Bergles, D.E. and Richardson, W.D. (2015). Oligodendrocyte development and plasticity. Cold Spring Harb Perspect Biol. 8 (2).

Betizeau, M., Cortay, V., Patti, D., Pfister, S., Gautier, E., Bellemin-Menard, A., Afanassieff, M., Huissoud, C., Douglas, R.J., Kennedy, H., et al. (2013) Precursor diversity and complexity of lineage relationships in the outer subventricular zone of the primate. Neuron 80 (2), 442-457.

Bhaduri, A., Andrews, M.G., Leon, W.M., Jung, D., Shin, D., Allen, D., Jung, D., Haeussler, M., Salma, J., Pollen, A.A., et al. (2020). Cell stress in cortical organoids impairs molecular subtype specification. Nature 578, 142-148.

Cai, J., Qi, Y., Hu, X., Tan, M., Liu, Z., Zhang, J., Liu, Q., Sander, M., and Qiu, M. (2005). Generation of oligodendrocyte precursor cells form mouse dorsal spinal cord independent of Nkx6 regulation and Shh signaling. Neuron 45, 41-53.

da Cunha Santos, G., Shepherd, F.A. and Tsao, M.S. (2011). EGFR mutations and lung cancer. Annu Rev Pathol. 6, 49-69.

Dugas, J.C., and Emery, B. (2013). Purification and culture of oligodendocyte lineage cells. Cold Spring Harb Protoc. 13 (9), 810-814.

Emery, B. and Lu, Q.R. (2015). Transcriptional and epigenetic regulation of oligodendrocyte development and myelination in the central nervous system. Cold Spring Harb Perspect Biol. 7 (9).

Eskilsson, E., Rosland, G.V., Solecki, G., Wang, Q., Harter, P.N., Graziani, G., Verhaak, R.G.W., Winkler, F., Bjerkvig, R., Miletic, H. (2018). EGFR heterogeneity and implications for therapeutic intervention in glioblastoma. Neuro Oncol. 20 (6), 743-752.

Fancy, S.P., Chan, J.R., Baranzini, S.E., Franklin, R.J., and Rowitch, D.H. (2011). Myelin regeneration: a recapitulation of development? Annu Rev Neurosci. 34, 21-43.

Fernandez, V., Llinares-Benadero, C., and Borrell, V. (2016). Cerebral cortex expansion and folding, what have we learned? EMBO J. 35 (10), 1021-1044.

Fietz, S.A., Kelava, I., Vogt, J., Wilsch-Brauninger, M., Stenzel, D., Fish, J.L., Corbeil, D., Riehn, A., Distler, W., Nitsch, R., and Huttner, W.B. (2010). OSVZ progenitors of human and ferret neocortex are epithelial-like and expand by integrin signaling. Nat Neurosci. 13 (6), 690-699.

Fish, J.L., Dehay, C., Kennedy, H., and Huttner, W.B. (2008). Making bigger brains-the evolution of neural-progenitor-cell dividion. J.Cell Sci. 121, 2783-2793.

Fogarty, M., Richardson, W.D., and Kessaris, N. (2005). A subset of oligodendrocytes generated from radial glia in the dorsal spinal cord. Development 132, 1951-1959.

Fuerst, P.G., Koizumi, A., Masland, R.H., and Burgess, R.W. (2008). Neurite arborization and mosaic spacing in the mouse retina require DSCAM. Nature 451 (7177), 470-474.

Gertz, C.C. and Kriegstein, A.R. (2015). Neuronal migration dynamics in the developing ferret cortex. J Neurosci. 35 (42), 14307-14315.

Hansen, D.V., Lui, J.H., Parker, P.R., and Kriegstein, A.R. (2010). Neurogenic radial glia in the outer subventricular zone of human neocortex. Nature 464 (7288), 554-561.

Hattori, D., Millard, S.S., Wojtowicz, W.M., and Zipursky, S.L. (2008). Dscam-mediated cell recognition regulates neural circuit formation. Annu Rev Cell Dev Biol. 24, 597-620.

Hill, R.A., Patel, K.D., Goncalves, C.M., Grutzendler, J., and Nishiyama, A. (2014). Modulation of oligodendrocyte generation during a critical temporal window after NG2 cell division. Nat Neurosci. 17 (11), 1518-1527.

Hughes, E.G., Kang, S.H., Fukaya, M., and Bergles, D.E. (2013). Oligodendrocyte progenitors balance growth with self-repulsion to achieve homeostasis in the adult brain. Nat Neurosci. 16 (6), 668-676.

Hu, W.F., Chahrour, M.H., and Walsh, C.A. (2014). The diverse genetic landscape of neurodevelopmental disorders. Annu Rev Genomics Hum Genet. 15, 195-213.

Jakovceviki, I., and Zecevic, N., (2005). Sequence of oligodendrocyte development in the human fetal telencephalon. Glia 49 (4), 480-491.

Kessaris, N., Fogarty, M., Lannarelli, P., Grist, M., Wegner, M., and Richardson, W.D. (2006). Competing waves of oligodendrocytes in the forebrain and postnatal elimination of an embryonic lineage. Nat Neurosci. 9 (2), 173-179.

La Manno, G., Gyllborg, D., Codeluppi, S., Nishimura, K., Salto, C., Zeisel, A., Borm, L.E., Stott, S.R.W., Teledo, E.M., Vellaescusa, J.C., et al. (2016) Molecular diversity of midbrain development in mouse, human, and stem cells. Cell 167 (2), 566-58.

Lefebvre, J.L., Kostadinov, D., Chen, W.V., Maniatis, T., and Sanes, J.R. (2012). Protocadherins mediate dendritic self-avoidance in the mammalian nervous system. Nature 488 (7412), 517-521.

Lui, J.H., Hansen, D.V., and Kriegstein, A.R. (2011). Development and evolution of the human neocortex. Cell 146 (1), 18-36.

Marques, S., Zeisel, A., Codeluppi, S., van Bruggen, D., Mendanha Falcao, A., Xiao, L., Li, H., Haring, M., Hochgerner, H., Romanov, R.A., et al. (2016). Oligodendrocyte heterogeneity in the mouse juvenile and adult central nervous system. Science 352 (6291), 1326-1329.

Marques, S., van Bruggen, D., Vanichkina, D.P., Floriddia, E.M., Munguba, H., Varemo, L., Giacomello, S., Falcao, A.M., Meijer, M., Bjorklund, A.K., et al. (2018). Transcriptional convergence of oligodendrocyte lineage progenitors during development. Dev Cell. 46 (4), 504-517.

Mo, Z. and Zecevic, N. (2009). Human fetal radial glia cells generate oligodendrocytes in vitro. Glia 57, 490-498.

Noctor, S.C., Flint, A.C., Weissman, T.A., Dammerman, R.S., and Kriegstein, A.R. (2001). Neurons derived from radial glia cells establish radial units in neocortex. Nature 409, 714-720.

Nonaka-Kinoshita, M., Reillo, I., Artegiani, B., Martinez-Martinez, M.A., Nelson, M., Borrell, V., and Calegari, F. (2013). Regulation of cerebral cortex size and folding by expansion of basal progenitors. EMBO J. 32 (13), 1817-1828.

Nowakowski, T.J., Bhaduri, A., Pollen, A.A., Alvarado, B., Mostajo-Radji, M.A., Di Lullo, E., Haeussler, M., Saudoval-Espinosa, C., Liu, S.J., Velmeshev, D., et al. (2017). Spatiotemporal gene expression trajectories reveal developmental hierarchies of the human cortex. Science 358 (6368), 1318-1323.

Pollen, A.A., Nowakowski, T.J., Chen, J., Retallack, H., Sandoval-Espinosa, C., Nicholas, C.R., Shuga, J., Liu, S.J., Oldham, M.C., Diaz, A., et al. (2015). Molecular identity of human outer radial glia during cortical development. Cell 163 (1), 55-67.

Pringle, N.P. and Richardson, W.D. (1993). A singularity of PDGFRa expression in the dorsoventral axis of the neural tube may define the origin of the oligodendrocyte lineage. Development 117, 525-533.

Qiu, X., Mao, Q., Tang, Y., Wang, L., Chawla, R., Pliner, H.A., and Trapnell, C. (2017). Reversed graph embedding resolves complex single-cell trajectories. Nat Methods. 14 (10), 979-982.

Rakic, P. (2009). Evolution of the neocortex, a perspective from developmental biology. Nat Rev Neurosci. 10 (10), 724-735.

Rakic, S. and Zecevic N. (2003). Early oligodendrocyte progenitor cells in the human fetal telencephalon. Glia 41, 117-127.

Rash, B.G., Duque, A., Morozov, Y.M., Arellano, J.I., Micali, N., and Rakic, P. (2019). Gliogenesis in the outer subventricular zone promotes enlargement and gyrification of the primate cerebrum. Proc Natl Acad Sci USA. 116 (14), 7089-7094.

Rowitch, D.H. and Kriegstein, A.R. (2010). Developmental genetics of vertebrate glia-cell specification. Nature 468 (7321), 214-222.

Simons, M. and Nave, K.A. (2015). Oligdendrocytes, Myelination and axonal support. Cold Spring Harb Perspect Biol. 8(1).

Smart, I.H., Dehay, C., Giroud, P., Berland, M., and Kennedy, H. (2002). Unique morphological features of the proliferative zones and postmitotic compartments of the neural epithelium giving rise to striate and extrastriate cortex in the monkey. Cereb.Cortex 12, 37-53.

Subramanian, L., Bershteyn, M., Paredes, M.F., and Kriegstein, A.R. (2017). Dynamic behavior of human neuroepithelial cells in the developing forebrain. Nat Commun. 8, 14167.

Taverna, E., Gotz, M., and Huttner, W.B. (2014). The cell biology of neurogenesis, toward an understanding of the development and evolution of the neocortex. Annu Rev Cell Dev Biol. 30, 465-502.

Trapnell C., Cacchiarelli, D., Grimsby, J., Pokharel, P., Li, S., Morse, M., Lennon, N.J., Mikkelsen, T.S., and Rinn, J.L. (2014). The dynamics and regulators of cell fate decisions are revealed by pseudotemporal ordering of single cells. Nat Biotechnol. 32 (4), 381-386.

Vallstedt, A., Klos, J.M., and Ericson, J. (2005). Multiple dorsoventral origins of oligodendrocyte generation in the spinal cord and hindbrain. Neuron 45, 55-67.

Walsh, C.A. (1999). Genetic malformations of the human cerebral cortex. Neuron 23 (1), 19-29.

Warf, B.C., Fok-Seang, J.m and Miller, R.H. (1991). Evidence for the ventral origin of oligodendrocyte precursors in the rat spinal cord. J Neurosci. 11, 2477-2488.

Yu, Y.C., Bultje, R.S., Wang, X., and Shi, S.H. (2009). Specific synapses develop preferentially among sister excitatory neurons in the neocortex. Nature 458, 501-504.

Zecevic, N., Chen, Y., and Filipovic, R. (2005). Contributions of cortical subventricular zone to the development of the human cerebral cortex. J.Comp.Neurol. 491, 109-122.

Zhang, K. and Sejnowski, T.J. (2000). A universal scaling law between gray matter and white matter of cerebral cortex. Proc Notl Acad Sci USA. 97 (10), 5621-5626.

Zhu, X., Hill, R.A., Dietrich, D., Komitova, M., Suzuki, R., and Nishiyama, A. (2011). Age-dependent fate and lineage restriction of single NG2 cells. Development 138, 745-753.